

A constrained Potts antiferromagnet model with an interface representation

J. K. BURTON JR. and C. L. HENLEY

Department of Physics, Cornell University

Ithaca, NY 14853-2501, U. S. A.

Abstract

We define a four-state Potts model ensemble on the square lattice, with the constraints that neighboring spins must have different values, and that no plaquette may contain all four states. The spin configurations may be mapped into those of a 2-dimensional interface in a 2+5 dimensional space. If this interface is in a Gaussian rough phase (as is the case for most other models with such a mapping), then the spin correlations are critical and their exponents can be related to the stiffness governing the interface fluctuations. Results of our Monte Carlo simulations show height fluctuations with an anomalous dependence on wavevector, intermediate between the behaviors expected in a rough phase and in a smooth phase; we argue that the smooth phase (which would imply long-range spin order) is the best interpretation.

1 Introduction

A number of discrete spin models with highly degenerate ground states have critical ground state ensembles: these include the triangular Ising antiferromagnet with spin 1/2 (Wannier, 1950; Nienhuis *et al.*, 1984) or with general spin (Lipowski *et al.*, 1995; Zeng and Henley, 1997), the three-state antiferromagnetic Potts model on the square lattice or equivalently the six-vertex model (Lieb and Wu, 1972; Kolafa, 1984; Wang *et al.*, 1989; Wang *et al.*, 1990; Park and Widom, 1989; Ferreira and Sokal, 1995), the three-state Potts antiferromagnet on the Kagomé lattice (Baxter, 1970), coverings of the square lattice by dimers of one color (Fisher and Stephenson, 1963) or of two colors (Raghavan *et al.*, 1997), and the four-coloring of the edges of the square lattice (Read, 1992).

All known models of this type can be mapped, configuration by configuration, to configurations of integer-valued ‘heights’ $\mathbf{z}(\mathbf{x})$ (van Beijeren, 1977; Blöte and Hilhorst, 1982; Kolafa, 1984; Zheng and Sachdev, 1989; Levitov, 1990; Huse and Rutenberg, 1992; Kondev and Henley, 1995b; Kondev and Henley, 1996); we will call models with this property ‘height models’. We can interpret $\mathbf{z}(\mathbf{x})$ as parametrizing a surface, which (in most of the above cases) turns out to be in its *rough* phase, described by a gradient-squared free energy at long wavelengths. By standard methods, this corresponds to algebraically decaying spin-spin correlations. (See e.g. Nelson (1983) and Nienhuis (1987); we review the derivation in Sec. 2). The exponents may be calculated from the stiffness constant in the long-wavelength Gaussian free energy, and indeed the most accurate way to determine the exponents is by directly determining this stiffness constant from the mean-square fluctuations of the Fourier transform of $\mathbf{z}(\mathbf{x})$, as measured in Monte Carlo simulations (Kondev and Henley, 1995b; Raghavan *et al.*, 1997; Zeng and Henley, 1997). It can be seen that the spirit of this ‘height model’ approach is geometrical: spin fluctuations are visualized as undulations of an interface model, and critical exponents are obtained through computations of reciprocal lattice vectors in a high dimensional lattice.

The height model we introduce here is a new way of generalizing the three-state Potts

antiferromagnet (AFM) on the square lattice to general q (and particularly to $q = 4$). Recall that the three-state Potts AFM is in a ground state if and only if the four spins around every plaquette are (ABAB), (ABCB), or a configuration related to these by symmetry. The usual q -state Potts AFM with $q > 3$ allows an additional kind of plaquette configuration in the ground state, of type (ABCD), and it turns out that this excludes any height representation, which was responsible for the interesting critical properties of the $q = 3$ case. (Indeed, the Potts AFM with $q > 3$ has exponential rather than power-law decay of correlations (Grest and Banavar, 1981).) Therefore, our model excludes the additional kind of plaquette so as to keep the height representation. We call such a model a ‘constrained Potts antiferromagnet’ (CPAFM). Our motivation to study this model is that the height space (in which the \mathbf{z} vectors live) has an especially high dimension (five), and hence might exhibit a new universality class.

In the remainder of this paper, we present a study of the 4-state CPAFM model on the square lattice. First, in Sec. 2, we review the basic ideas of height models (using the 3-state Potts AFM as a specific example). In particular, we explain how to express a spin operator in terms of the height correlation function. In Sec. 3 we carry this out for the more complicated case of the 4-state CPAFM, presenting the height mapping of spin configurations and the height representation of spin operators. Sec. 4 describes the cluster Monte Carlo algorithm needed for studying such models. We present the simulation results, and discuss their implications for whether the system is in a critical or a long-range-ordered state, in Sec. 5. Finally, Sec. 6 summarizes our results in the context of related models.

In the present paper, we have considered only the zero temperature behavior. At small nonzero temperatures, there are rare plaquettes where the constraint rule is violated. Each such point corresponds to a vortex-like defect (a dislocation) in $\mathbf{z}(\mathbf{x})$. In other height models, such defects are associated with further interesting exponents (Kondev and Henley, 1996). Formulas for these exponents (assuming a rough surface) would be straightforward to derive for the CPAFM model as an extension of Sec. 3.

2 Example height model: The 3-state Potts AFM

This section is a pedagogical introduction to some basic concepts and methods which are valid for all “height models”. Of these, we chose the three-state Potts antiferromagnet (AFM) on the square lattice (see Figure 1) as the example model for its obvious analogies to the more elaborate 4-state model of Sec. 3. (These analogies also led us to select it for numerical comparisons). Furthermore, this model had never been explicitly analyzed using the geometrical “height-model” language¹, except in the poorly-known simulation paper of Kolafa (1984).

As already noted, a configuration is a ground state if and only if each plaquette is assigned either two or three distinct spins, with like spins situated on opposite corners of the plaquette. Our object is to compute the critical exponent governing the decay of the correlation function of various operators. The steps to this are, first, to map the spins to a height representation described by a gradient-squared free energy, which allows us to compute correlations of the height variables (subsec. 2.1 below, in particular Eq. (2.5)); second, to relate the spin operators to the height variables (subsec. 2.2 and 2.3 below). The same steps would be used for any other height model (Kondev and Henley, 1995a; Kondev and Henley, 1995b; Kondev and Henley, 1996; Raghavan *et al.*, 1997) and in particular for the 4-state CPAFM (in Sec. 3, below).²

In view of the application to a multi-dimensional height variable in Sec. 3, the most important new concepts here are the three lattices associated with height space, defined in Subsec. 2.4. In addition, the concept of ‘ideal state’ is introduced in Sec. 2.2 which eases

¹The triangular Ising antiferromagnet *was* so analyzed by Nienhuis *et al.* (1984).

²The height map described in subsec. 2.1 also works for the $q = 3$ Potts AFM on a simple cubic lattice. That model has long-range order in the ground state ensemble (Banavar *et al.*, 1980) as would be expected from the three-dimensional version of our arguments below. At higher temperatures it almost exhibits continuous symmetry behavior (Gottlob and Hasenbusch, 1994; Kolesik and Suzuki, 1995). It is intriguing, then, to speculate whether its coarse-grained height variable becomes the angle of an XY-model, as does happen in the two-dimensional case we describe in this section.

(and geometrizes) the determination of the G vector of a given operator.

The *results* of this section were already derived by den Nijs *et al.* (1982), but those authors had a different focus: they downplayed the exact mapping to height variables, while emphasizing the application of results from renormalization group theory and from exact solutions of the eight-vertex model. (For our results, a more elementary theoretical level will suffice.) However, once the height-space reciprocal lattice vector G is identified for a particular operator, the scaling indices $\eta(G)$ are found here (see Sec. 2.3) exactly as in den Nijs *et al.* (1982).

2.1 Height mapping

For each ground state configuration, we define a height function $z(\mathbf{x})$ such that the difference in height, Δz , in going from one site to a neighboring site is $+1$ if the pair of spins are in the same order as in $A \rightarrow B \rightarrow C \rightarrow A$ and is -1 if they are in the reverse order. In this way we have a height $z(\mathbf{x})$ uniquely assigned to each site \mathbf{x} once the height at any particular site is specified (see Figure 1(b)). This $z(\mathbf{x})$ is well-defined (since the sum of Δz around any closed loop is zero) for any ground state.

We can coarse-grain the microscopic $z(\mathbf{x})$ to obtain the macroscopic height $h(\mathbf{x})$. We now postulate an effective elastic free energy of the form

$$F = \int d\mathbf{x} \frac{1}{2} K |\nabla h(\mathbf{x})|^2, \quad (2.1)$$

where K is a stiffness constant. Writing (2.1) in terms of $\tilde{h}(\mathbf{q})$, the Fourier transform of $h(\mathbf{x})$, gives

$$F = \sum_{\mathbf{q}} \frac{1}{2} K |\mathbf{q}|^2 |\tilde{h}(\mathbf{q})|^2, \quad (2.2)$$

where the Fourier transform is normalized as

$$h(\mathbf{x}) = \frac{1}{\sqrt{N}} \sum_{\mathbf{q}} e^{i\mathbf{q}\cdot\mathbf{x}} \tilde{h}(\mathbf{q}) \quad (2.3)$$

and N is the number of sites in the lattice. All sums over q run over the first Brillouin zone.

Hence, the partition function is a product of independent Gaussians and the fluctuations in $\tilde{h}(\mathbf{q})$ are given by

$$\langle |\tilde{h}(\mathbf{q})|^2 \rangle = \frac{1}{K|\mathbf{q}|^2}. \quad (2.4)$$

Fourier transforming back to real space shows that the height correlation function is

$$\langle |h(\mathbf{x}') - h(\mathbf{x})|^2 \rangle \approx \frac{1}{\pi K} \log r + C, \quad (2.5)$$

where $r \equiv |\mathbf{r}| \equiv |\mathbf{x}' - \mathbf{x}|$ is assumed to be large and C is a constant. Models for which $\langle |h(\mathbf{x}') - h(\mathbf{x})|^2 \rangle$ diverges as $r \rightarrow \infty$ (as in (2.5)) are termed “rough.” Therefore, models for which (2.1) is valid (with finite, nonzero stiffness K) are rough, as is the 3-state Potts AFM.

2.2 Ideal states

The first step in relating spin operators to heights is to define a set of reference states, called ‘ideal states’, such that the spin, $\sigma(\mathbf{x})$, on site \mathbf{x} is a function of the coarse-grained height at \mathbf{x} . Ideal states are configurations which (i) consist of a periodic pattern of spins, (ii) have zero macroscopic height gradient ∇h (and are therefore called ‘flat’), and (iii) have maximal entropy for local fluctuations. In general, “ideal states” make it convenient to identify the height-space reciprocal lattice vector (see Subsec. 2.3, below) which is associated with the locking operator and with spin operators of interest (see Subsec. 2.4).

The ideal states for the 3-state Potts AFM are the A B/C state (left part of Figure 1(a)) and the others equivalent to it by symmetry; in our nomenclature the labels refer to the even and odd sublattices, respectively, and a label ‘B/C’ indicates a disordered site with spin having equal probability of B or C. A first guess for an ideal state might have been the AB state (center part of Figure 1(a)), which is clearly periodic and flat. However, the number of states ‘close to’ the AB state is less than the number of states close to the typical A B/C state. (Here distance between states is measured by the number of spin flips required to convert one into the other.) Hence, the AB state is not an ideal state, but rather a transition state between A B/C and C/A B states.

All the sites in the completely ordered sublattice of an ideal state (e.g. the even sites in an A B/C state) clearly have the same microscopic height $z = z_0$. The values of z on the sites in the disordered lattice are $z_0 \pm 1$, with the sign depending on the particular value of the spin on that site. Since a disordered site is equally likely to have either of the two possible spins, it is clear that the macroscopic height of the ideal state is $h = z_0$.

We expect a typical ground state configuration to consist primarily of macroscopic domains of ideal states, separated by thin walls of transition states. The value of h within a domain is simply the value of z on the disordered sublattice of the domain. Therefore, the macroscopic height difference, Δh , between two ideal domains can be calculated by finding the net height change along a path of neighboring sites connecting a site \mathbf{x} in the ordered sublattice of the first domain with a site \mathbf{x}' in the ordered sublattice of the second domain:

$$\Delta h = \sum_{i=0}^{n-1} \Delta z(\sigma(\mathbf{x}_i), \sigma(\mathbf{x}_{i+1})) = \sum_{i=0}^{n-1} \Delta z(\sigma_i, \sigma_{i+1}), \quad (2.6)$$

where n is the number of bonds in the chosen path connecting \mathbf{x} to \mathbf{x}' , \mathbf{x}_i and \mathbf{x}_{i+1} are nearest neighbors for $i = 0$ to $n - 1$, $\sigma_i = \sigma(\mathbf{x}_i)$ for $i = 0$ to n , $\mathbf{x}_0 = \mathbf{x}$, and $\mathbf{x}_n = \mathbf{x}'$. Note that n is even if the same sublattice is ordered in both domains, and n is odd if opposite sublattices are ordered in the two domains. It is not difficult to show (see Appendix B) that the macroscopic height difference between two domains is uniquely determined (modulo 6) by the identities of the ideal states in the two domains. Whether two patches of (say) A B/C domain have the same height, or heights which differ by ± 6 (or more), is not arbitrary but depends on the configurations between the domains. For example, if we follow a path through a succession of domains A B/C, C/A B, C A/B, B/C A, A/B C, and back to A B/C, each has a macroscopic height h larger by 1 than the previous domain, so that the second A B/C domain has a height that is 6 greater than the first A B/C domain. (See Figure 2(a).) Once the microscopic height on a particular site is set, the ideal state pattern (and in particular the spin value on the ordered sublattice) within every ideal-state domain can be identified uniquely from its height h .

2.3 Correlation exponents

Our goal is to compute the correlation function of a given local operator $O(\mathbf{x})$, which is some function of the spins $\sigma(\mathbf{x}')$ for \mathbf{x}' in a neighborhood of \mathbf{x} . To accomplish this, we must first convert this operator from a function of the local spin variables to a function of the local height variables. Namely, each site belongs to a domain of some ideal state; the spin variable on that site is determined by the ideal state label of that domain, and (as emphasized in Subsec. 2.2) every ideal state is labeled unambiguously by its height h .

Since the periodicity of the spin arrangement in each ideal state divides the lattice into ‘even’ and ‘odd’ sublattices, any local operator $O(\mathbf{x})$ will have similar periodicity and dependence on which sublattice \mathbf{x} is in:

$$O(\mathbf{x}) = F_O^{\epsilon(\mathbf{x})}(h), \quad (2.7)$$

where $\epsilon(\mathbf{x})$ is the parity of site \mathbf{x} ($\epsilon(\mathbf{x}) = 1$ if \mathbf{x} is in the even sublattice and $\epsilon(\mathbf{x}) = -1$ if \mathbf{x} is in the odd sublattice). In addition, since $O(\mathbf{x})$ depends on h only through its dependence on the ideal state label, we have

$$F_O^{\epsilon(\mathbf{x})}(h) = F_O^{\epsilon(\mathbf{x})}(h + a_\perp), \quad (2.8)$$

where a_\perp is any integer multiple of 6.

In light of (2.7) and (2.8) the function $F_O^{\epsilon(\mathbf{x})}$ can be expanded as a Fourier series:

$$O(\mathbf{x}) = F_O^{\epsilon(\mathbf{x})}(h) = \sum_G O_G^{\epsilon(\mathbf{x})} e^{iGh}, \quad (2.9)$$

where G ranges over the integer multiples of $2\pi/6$. From (2.9) we conclude that the correlations of $O(\mathbf{x})$ satisfy

$$\langle O(\mathbf{x})O(\mathbf{x}') \rangle = \sum_{G,G'} O_G^{\epsilon(\mathbf{x})} O_{G'}^{\epsilon(\mathbf{x}')*} \langle e^{i(Gh-G'h')} \rangle, \quad (2.10)$$

where h is the height at \mathbf{x} , h' is the height at \mathbf{x}' , and $\langle \dots \rangle$ denotes the average over allowed configurations. Note that

$$\langle e^{i(Gh-G'h')} \rangle = \langle e^{iG(h-h')} e^{i(G-G')h'} \rangle = \langle e^{iG(h-h')} \rangle \langle e^{i(G-G')h'} \rangle, \quad (2.11)$$

where the second equality follows because $(h - h')$ is independent of h' . But $\langle e^{i(G-G')h'} \rangle = \delta_{G,G'}$, so that substituting (2.11) into (2.10) gives

$$\langle O(\mathbf{x})O(\mathbf{x}') \rangle = \sum_G O_G^{\epsilon(\mathbf{x})} O_G^{\epsilon(\mathbf{x}')*} \langle e^{iG(h-h')} \rangle. \quad (2.12)$$

Since $\{\tilde{h}(\mathbf{q})\}$ are Gaussian distributed, so is $h(\mathbf{x}) - h(\mathbf{x}')$. Moreover, $\langle h(\mathbf{x}) - h(\mathbf{x}') \rangle$ is clearly zero. Hence, we can use (2.5) to show

$$\langle e^{iG(h-h')} \rangle = e^{-\frac{1}{2}G^2 \langle |h-h'|^2 \rangle} \approx c(|G|) r^{-\eta_G} \text{ as } r \rightarrow \infty, \quad (2.13)$$

where

$$\eta_G = \frac{G^2}{2\pi K} \quad (2.14)$$

and $c(|G|) = e^{-G^2 C/2} > 0$. With (2.13), equation (2.12) becomes

$$\begin{aligned} \langle O(\mathbf{x})O(\mathbf{x}') \rangle &\approx \sum_G c(|G|) O_G^{\epsilon(\mathbf{x})} O_G^{\epsilon(\mathbf{x}')*} r^{-\eta_G} \\ &\approx f(\epsilon(\mathbf{x}), \epsilon(\mathbf{x}')) r^{-\eta}, \end{aligned} \quad (2.15)$$

where

$$\eta = \min \left\{ \eta_G : G = \frac{2\pi n}{6}; n \in \mathbb{N}; O_G^{+1} \text{ or } O_G^{-1} \text{ is nonzero} \right\} \equiv \eta_{G_0}, \quad (2.16)$$

$c = c(G_0)$, and $f(\epsilon, \epsilon') = 2c \operatorname{Re} \left\{ O_{G_0}^{\epsilon} O_{G_0}^{\epsilon'*} \right\}$. Note that G_0 is the smallest positive wavevector where the (height space) Fourier transform is nonzero. Also, $f(\epsilon, \epsilon')$ is not identically zero if and only if at least one of O_G^{+1} and O_G^{-1} is nonzero – and this is guaranteed by (2.16). Strictly speaking, equation (2.15) is valid as written only if $f(\epsilon, \epsilon')$ is nonzero for all four possible argument combinations. If this is not true, then for $(\mathbf{x}, \mathbf{x}')$ where $f(\epsilon(\mathbf{x}), \epsilon(\mathbf{x}')) = 0$ we should interpret (2.15) as saying $\langle O(\mathbf{x})O(\mathbf{x}') \rangle \ll r^{-\eta}$.

In any case, we see that an effective elastic free energy of the form (2.1) implies that correlations in any (nontrivial) operator decay algebraically – i.e., there is quasi-long-range order. Moreover, once the stiffness K is known, the decay exponent η for correlations in any operator can be determined from (2.14) and (2.16). Thus, all correlation exponents are known once any of them is determined.

2.4 Specific operators

Now we are ready to predict (in terms of the stiffness K) the exponents for explicit operators in the 3-state Potts AFM model. To do this, one should (for a given site \mathbf{x}) make a plot of the value of $O(\mathbf{x})$ as a function of the coarse-grained height h that labels the ideal state, as shown in Fig. 2; the Fourier components (as in Eq. 9) can then be read off, along with the coefficients $O_G^{\epsilon(\mathbf{x})}$ (which are not usually needed).

In order to define the operators, it is helpful to represent the spin state on each site by a unit vector $\mathbf{m}(\mathbf{x})$ in the plane, pointing at angles 0 , $2\pi/3$, and $4\pi/3$, for spin states A, B, and C, respectively. We must first identify the value of G_O corresponding to a given operator.

The *staggered* magnetization operator $\mathbf{m}^s(\mathbf{x}) \equiv \epsilon(\mathbf{x})\mathbf{m}(\mathbf{x})$ is the order parameter since it distinguishes among the 6 ideal states and also has the maximum height-space period of 6, as shown in Figure 2(b). Thus, the minimizing wavevectors in (2.16) are $G_S = \pm\frac{2\pi}{6}$. The value $\eta_S = \frac{\pi}{18K}$ then follows directly from (2.14). Wang *et al.* (1989) found η_S numerically from Monte Carlo simulations. The exponents were obtained analytically by Park and Widom (1989), using the exact mapping of the 3-state Potts AFM to the 6-vertex model and the known exact solution of the latter. They found the free energy cost of ‘step’ boundary conditions, forcing $\Delta h = \pm 2$ across the system, to be $\Delta F = 2\pi/6L$; via conformal invariance this implied $\eta_S = 1/3$. Given that this is a height model, one could instead directly extract the stiffness $K = \pi/6$ by inserting the forced tilt $\Delta h/L$ into (2.1) (which gives $F = K(\Delta h)^2/2L$).

The ideal states are ‘ferrimagnetic’ – i.e., they each have a net magnetization \mathbf{M} ; this operator has a height-space period of 3 (see Figure 2(b)). Therefore, $G_M = \pm 2\pi/3 = 2G_S$ and $\eta_M = 4\eta_S = 4/3$. The ferromagnetic exponent η_M seems to be considered explicitly only by den Nijs *et al.* (1982), who used a Coulomb-gas approach very similar to ours to reach the same conclusions. This exponent is relevant and could easily be measured in simulations, but this has apparently never been implemented.

An ideal state can have either the even or odd sublattice as the ordered one. These

possibilities can be distinguished by the sign of the operator $P(\mathbf{x}) = \frac{1}{4}\epsilon(\mathbf{x}) \sum_{\text{n.n.n. } \mathbf{x}'} \delta_{\sigma(\mathbf{x}),\sigma(\mathbf{x}')}$, where the sum is over \mathbf{x}' which are second neighbors with \mathbf{x} . The height-space period of this operator is clearly 2 and, hence, $G_{sub} = \pm 2\pi/2$. The exponent for this operator is irrelevant for the (ground state) 3-state Potts AFM model.

At this point we may identify three one-dimensional lattices which appear in the height representation of the three-state Potts AFM. First, the “repeat lattice” in height space has period 6, because (as noted in Sec. 2.2) the spin pattern as a function of h repeats itself with that period. Secondly, the “equivalence lattice” has period 1, since $h \rightarrow h + 1$ is induced by a global permutation of Potts spins to give a symmetry-equivalent state. Finally, the “height space reciprocal lattice” is dual to the repeat lattice and thus has period $2\pi/6$ for this model; it is a general fact about height models that the allowed G values (see Sec. 2.3) belong to the reciprocal lattice. These lattices were not defined in prior applications of height models, since they are rather trivial in one dimension; they begin to become useful when one wants to make a systematic comparison between different height models, and they are quite essential in dealing with multi-dimensional height models, as in the next section.

3 The 4-state constrained Potts AFM

A more complicated model with a height mapping is the 4-state constrained Potts antiferromagnetic (CPAFM) model on the square lattice (see Figure 3(a)). Now there are four possible spins – A, B, C, and D – and, on top of the antiferromagnetic nearest-neighbor constraint, there is the added constraint that no plaquette may contain more than 3 distinct spin states. In particular, as in the 3-state Potts AFM model, a configuration is a ground state if and only if each plaquette is assigned either two or three distinct spins, with like spins situated on opposite corners of the plaquette.

In this section, we will work through all the stages of analyzing this model via its height representation. These are (i) discovering all vector components of the height representation; (ii) determining the generic elastic theory; (iii) mapping the ideal-states as a point set in height space (associated with this is the “repeat lattice”); (iv) evaluating the height-space reciprocal lattice vectors, and finally the exponents, corresponding to the operators of interest.

3.1 Height mapping and elastic theory

Unlike in the 3-state case, height space for the 4-state CPAFM model is multidimensional. It has dimension $d^\perp = 5$ and can be viewed as the Cartesian product of a 3-dimensional ‘even’ height subspace and a 2-dimensional ‘odd’ height subspace. For these we shall sometimes use the notation $(a, b, c)_E \equiv (a, b, c, 0, 0)$ and $(a, b)_O \equiv (0, 0, 0, a, b)$.

The change in height in going from a site \mathbf{x} to a neighboring site \mathbf{x}' is $\mathbf{z}(\mathbf{x}') - \mathbf{z}(\mathbf{x}) = \Delta\mathbf{z} = \Delta\mathbf{z}^E \otimes \Delta\mathbf{z}^O$, where $\Delta\mathbf{z}^E \equiv (\Delta z_1, \Delta z_2, \Delta z_3)$ and $\Delta\mathbf{z}^O \equiv (\Delta z_4, \Delta z_5)$ are the even and odd height change functions, respectively. Here $\Delta\mathbf{z}^E = \Delta\mathbf{z}^E(\sigma(\mathbf{x}), \sigma(\mathbf{x}'))$ is a function only of the spins on the two sites and does not depend on which site belongs to which sublattice. On the other hand, $\Delta\mathbf{z}^O = \Delta\mathbf{z}^O(\epsilon(\mathbf{x}), \sigma(\mathbf{x}), \sigma(\mathbf{x}'))$ depends also on the parity $\epsilon(\mathbf{x})$ of the initial site but does not depend on which spin is on which site, i.e. $\Delta\mathbf{z}^O(\epsilon, \sigma, \sigma') = \Delta\mathbf{z}^O(\epsilon, \sigma', \sigma)$.

The identification of the correct height space is nontrivial: for example, had we simply

generalized the $q = 3$ case, we would have omitted the “odd” components, since the 3-state height variable is “even”. On the other hand, there is also a danger of including redundant height components. By redundant, we mean functions of the spins which are linear combinations of other height variables and of *bounded* functions of the spins. Appendix A gives the explicit construction of $\mathbf{z}(\mathbf{x})$ confirming the validity of its definition.

All values of $\Delta\mathbf{z}$ can be found from Table 1, which directly shows the value of $\Delta\mathbf{z}^E(\sigma, \sigma')$ for 12 of the 24 possible argument combinations and the value of $\Delta\mathbf{z}^O(\epsilon, \sigma, \sigma')$ for 24 of the 48 possible argument combinations. Values of $\Delta\mathbf{z}$ for the remaining argument combinations follow from $\Delta\mathbf{z}^E(\sigma, \sigma') = -\Delta\mathbf{z}^E(\sigma', \sigma)$ and $\Delta\mathbf{z}^O(\epsilon, \sigma, \sigma') = -\Delta\mathbf{z}^O(-\epsilon, \sigma', \sigma)$, which must hold for $\Delta\mathbf{z}(\mathbf{x})$ to be single-valued. Figure 3(b,c) shows an even and an odd component of height for the example configuration.

The primitive vectors for the ‘odd’ subspace, $(1, 0)_O$ and $(0, 1)_O$, have been chosen to have a 120° angle between them as is standard for a triangular lattice; thus the length of $(x_4, x_5)_O$ is $(x_4^2 + x_5^2 - x_4x_5)^{1/2}$.³ The *reciprocal* space ‘odd’ vectors, though, are defined so that (height) reciprocal-space $(1, 0)_O$ has a dot product with height-space $(1, 0)_O$ of unity, and with height-space $(0, 1)_O$ of zero; and such that reciprocal space $(1, 0)_O$ and $(0, 1)_O$ are 60° apart, so $(q_4, q_5)_O$ has length $(q_4^2 + q_5^2 + q_4q_5)^{1/2}$.

As with the 3-state model, $\mathbf{z}(\mathbf{x})$ is well-defined for any allowed spin configuration once its value at any particular site is specified, and we can coarse-grain the microscopic $\mathbf{z}(\mathbf{x})$ to obtain the macroscopic height $\mathbf{h}(\mathbf{x})$. The higher-dimensional analog of the elastic free energy in (2.1) is

$$F = \int d\mathbf{x} \frac{1}{2} \sum_{\alpha, \beta=1}^5 K_{\alpha\beta} \nabla h_\alpha \cdot \nabla h_\beta. \quad (3.1)$$

A detailed consideration of the symmetries of the square lattice was needed to verify that the coefficients in (3.1) are diagonal in the gradient indices. (In a general height model, they might depend on *four* indices, two for the gradients in addition to the two for height

³The symmetry in the definition of the ‘odd’ heights would be more evident using an alternative representation using three ‘odd’ components with the constraint $z_4 + z_5 + z_6 = 0$.

components.) The symmetries of the Potts spin further restrict the matrix $\mathbf{K} = (K_{\alpha\beta})$ to have the form

$$\mathbf{K} = \begin{pmatrix} K^{\text{E}} & 0 & 0 & 0 & 0 \\ 0 & K^{\text{E}} & 0 & 0 & 0 \\ 0 & 0 & K^{\text{E}} & 0 & 0 \\ 0 & 0 & 0 & K^{\text{O}} & -\frac{1}{2}K^{\text{O}} \\ 0 & 0 & 0 & -\frac{1}{2}K^{\text{O}} & K^{\text{O}} \end{pmatrix}, \quad (3.2)$$

where the even and odd height subspace stiffness constants, K^{E} and K^{O} , are as yet undetermined. (The ‘odd’ part of the density in (3.1) is just $\frac{1}{2}K^{\text{O}}|\nabla\mathbf{h}^{\text{O}}|^2$; the corresponding subblock in (3.2) looks nondiagonal due to our choice of primitive vectors for the ‘‘odd’’ subspace.) The generalization of (2.4) is

$$\langle \tilde{h}_\alpha(\mathbf{q}) \tilde{h}_\beta(\mathbf{q})^* \rangle = \frac{(\mathbf{K}^{-1})_{\alpha\beta}}{|\mathbf{q}|^2} \quad (3.3)$$

and, similarly, the analog of equation (2.5) is

$$\langle [h_\alpha(\mathbf{x}') - h_\alpha(\mathbf{x})] [h_\beta(\mathbf{x}') - h_\beta(\mathbf{x})] \rangle \approx \frac{(\mathbf{K}^{-1})_{\alpha\beta}}{\pi} \log(r) + C_{\alpha\beta}, \quad (3.4)$$

where $C_{\alpha\beta}$ is the $\alpha\beta$ component of a constant matrix \mathbf{C} . The term ‘rough’ is used to describe any height component, h_α , for which $\langle |h_\alpha(\mathbf{x}') - h_\alpha(\mathbf{x})|^2 \rangle \rightarrow \infty$ as $r \rightarrow \infty$. Hence, the even (odd) height components in the 4-state CPAFM model are rough if and only if K^{E} (K^{O}) is finite.

3.2 Ideal states

The ideal states in the 4-state CPAFM model are like those discussed in Sec. 2.2 for the 3-state model, except with three possible spins on each site in the disordered sublattice instead

of just two⁴ (see Figure 3(a), left part); for example, the ‘A B/C/D’ state with A on the even sublattice and disordered B/C/D on the odd sublattice. We shall sometimes use the abbreviated label ‘X’ for the disordered lattice, thus this ideal state is designated ‘AX’. Since there are two choices for which sublattice is ordered and four choices for which spin appears on the ordered sublattice, there are 8 ideal states.

All of our steps here are closely analogous to those for the 3-state model. All the sites in the completely ordered sublattice of an ideal state have the same macroscopic height $\mathbf{z} = \mathbf{z}_o$. The sites in the disordered lattice have height values $\mathbf{z}_o + \Delta\mathbf{z}$, where $\Delta\mathbf{z}$ has three possible values, corresponding to a step from the ordered spin to neighbors with the three possible kinds of spin state on the disordered sublattice. Since these $\Delta\mathbf{z}$ vectors add up to zero, and a disordered site is equally likely to have any of the three possible spin states, the macroscopic height of the ideal state is $\mathbf{h} = \mathbf{z}_o$.

The macroscopic height difference between two ideal domains can be calculated by finding the height change along a path of neighboring sites connecting a site \mathbf{x} in the ordered sublattice of the first domain to a site \mathbf{x}' in the ordered sublattice of the second domain. The generalization of equation (2.6) is simply

$$\Delta\mathbf{h} = \sum_{i=0}^{n-1} \Delta\mathbf{z}(\epsilon(\mathbf{x}_i), \sigma(\mathbf{x}_i), \sigma(\mathbf{x}_{i+1})) = \sum_{i=0}^{n-1} \Delta\mathbf{z}(\epsilon_i, \sigma_i, \sigma_{i+1}). \quad (3.5)$$

Note that now we must keep track of the site’s parity $\epsilon(\mathbf{x})$ in addition to the sequence of spins encountered. Altering this parity leaves $\Delta\mathbf{h}^E$ unchanged while causing $\Delta\mathbf{h}^O$ to change sign.

The differences (3.5) allow us to map out the ideal-states graph for the 3-state CPAFM model, of which each node is the \mathbf{h} of the corresponding ideal state. Neighboring ideal states (those which differ by the minimum number of spin changes) such as AX and XB are related

⁴This is like the intermediate-temperature state in the *unconstrained* 4-state Potts AFM (Grest and Banavar, 1981); however, the low-temperature behavior of that model may be better described by two states disordered on the even sublattice and the other two spin states on the odd sublattice (compare Banavar *et al.* (1980)).

by a $\Delta\mathbf{h}$ vector which is simply the $\Delta\mathbf{z}$ vector for the step AB, as listed in Table 1, and similarly for all other pairs. The ideal-state lattice is 3-coordinated (as is visible in either the ‘even’ or ‘odd’ projection) since, for any ideal state, there are 3 ways to make another ideal state with the minimal change. Ideal states related by exchanging even and odd sublattices turn out to be related by the shiftvectors in the upper half of Table 2, which are simply computed from Table 1; the parity ϵ is that of the first site in the string.

The ‘even’ space projection of the ideal-states graph is a ‘hydrogen peroxide lattice.’ (See Fig. 1 of Leu *et al.* (1969), and references therein. The Bravais lattice of this projection is body-centered cubic (bcc) with lattice constant 4. The crystallographic basis is 4 points per primitive bcc cell, at $[0, 0, 0]$ (assumed to represent the ideal state ‘AX’) and at $[0, 1, -1]$, $[1, 0, 1]$, and $[-1, -1, 0]$.⁵ All these points are equivalent by symmetry, and the nearest-neighbor bonds make 120° angles. Analogously, the ‘odd’ space projection is a honeycomb lattice with bonds of length $\sqrt{6}$.

3.3 Repeat lattice

Before considering operators as periodic functions of the height, we must understand the ‘repeat lattice’. In general this is defined as the set of possible macroscopic height differences between domains of the *same* ideal state in configurations allowed by the model. (Note the distinction from the Bravais lattice of the ideal-states graph.) Conversely, the macroscopic height difference $\Delta\mathbf{h}$ between domains of *different* ideal states can never belong to the repeat lattice. (This follows since $\Delta\mathbf{h}$ can never be zero in such a case, which can be checked explicitly for our models.) The repeat lattice of the 3-state Potts AFM is just the set of integer multiples of 6.

It can be checked (see Appendix B) that the repeat lattice of the 4-state CPAFM is a

⁵The same lattice is also known as the ‘Laves graph of degree three’ (Coxeter, 1955) and is the backbone of the minimal surface known as the ‘gyroid’ and found in bicontinuous systems (S. Milner, personal communication). It is interesting to compare this graph with Fig. 4 of Kondev and Henley (1995b), which is the three-dimensional ideal-states graph for a different 4-coloring model.

centered hyper-tetragonal lattice in 5-space generated by the vectors ⁶

$$\left\{ \mathbf{a}_i^\pm = \frac{1}{2} (\mathbf{a}_i^E \pm \mathbf{a}_i^O) : i \in \{1, 2, 3\} \right\}, \quad (3.6)$$

where

$$\begin{aligned} \mathbf{a}_1^E &= (8, 0, 0)_E & \mathbf{a}_2^E &= (0, 8, 0)_E & \mathbf{a}_3^E &= (0, 0, 8)_E \\ \mathbf{a}_1^O &= (0, 12)_O & \mathbf{a}_2^O &= (-12, 0)_O & \mathbf{a}_3^O &= (12, -12)_O. \end{aligned} \quad (3.7)$$

The vectors (3.6) span a space of only rank 5, as expected since $d^\perp = 5$. To represent the repeat lattice it is natural to choose the unit cell with \mathbf{a}_1^E , \mathbf{a}_2^E , \mathbf{a}_3^E , \mathbf{a}_1^O , and \mathbf{a}_2^O as edges along with the 8-point basis $\{A_1\mathbf{a}_1^+ + A_2\mathbf{a}_2^+ + A_3\mathbf{a}_3^+ : A_1, A_2, A_3 \in \{0, 1\}\}$.

3.4 Correlation exponents

As in the 3-state Potts AFM, the periodicity of the spin arrangement in each ideal state divides the lattice into even and odd sublattices, so that any local operator $O(\mathbf{x})$ has the form

$$O(\mathbf{x}) = F_O^{\epsilon(\mathbf{x})}(\mathbf{h}). \quad (3.8)$$

Again, $O(\mathbf{x})$ depends on height only in that it depends on the ideal state ensemble, so that

$$F_O^{\epsilon(\mathbf{x})}(\mathbf{h}) = F_O^{\epsilon(\mathbf{x})}(\mathbf{h} + \mathbf{a}^\perp), \quad (3.9)$$

where \mathbf{a}^\perp is any vector in the repeat lattice. We can therefore expand $F_O^{\epsilon(\mathbf{x})}$ in a Fourier series to obtain

$$O(\mathbf{x}) = F_O^{\epsilon(\mathbf{x})}(\mathbf{h}) = \sum_{\mathbf{G}} O_{\mathbf{G}}^{\epsilon(\mathbf{x})} e^{i\mathbf{G}\cdot\mathbf{h}}, \quad (3.10)$$

where the sum ranges over all \mathbf{G} in the repeat lattice's reciprocal lattice, which we henceforth call the 'height-space reciprocal lattice.' Proceeding as for the 3-state Potts AFM, but using (3.4) in place of (2.5), shows that

⁶These happen to be twice the vectors in the lower half of Table 2.

$$\langle O(\mathbf{x})O(\mathbf{x}') \rangle \approx F(\epsilon(\mathbf{x}), \epsilon(\mathbf{x}'))r^{-\eta} \text{ as } r \rightarrow \infty, \quad (3.11)$$

where

$$\eta = \min \{ \eta_{\mathbf{G}} : \mathbf{G} \neq 0; O_{\mathbf{G}}^{+1} \text{ or } O_{\mathbf{G}}^{-1} \text{ is nonzero} \}, \quad (3.12)$$

$$\eta_{\mathbf{G}} = \frac{1}{2\pi} \mathbf{G} \cdot \mathbf{K}^{-1} \mathbf{G}, \quad (3.13)$$

$F(\epsilon, \epsilon') = \sum_{\mathbf{G} \in G(\eta)} c(\mathbf{G}) \text{Re} \{ O_{\mathbf{G}}^{\epsilon} O_{\mathbf{G}}^{\epsilon' *} \}$, $c(\mathbf{G}) = e^{-\mathbf{G} \cdot \mathbf{C} \mathbf{G} / 2}$, and $G(\eta) = \{ \mathbf{G} : \eta_{\mathbf{G}} = \eta \}$. In each case \mathbf{G} is in the repeat lattice's reciprocal lattice. Again, equation (3.12) guarantees that $F(\epsilon, \epsilon')$ is not identically zero, and equation (3.11) should be read as $\langle O(\mathbf{x})O(\mathbf{x}') \rangle \ll r^{-\eta}$ if it happens that $F(\epsilon(\mathbf{x}), \epsilon(\mathbf{x}')) = 0$.

We see from the above and equation (3.2) that the 4-state CPAFM exhibits quasi-long-range order if and only if either K^E or K^O is finite. If they are both finite, the algebraic decay exponent for the correlations in any local operator can be determined once K^E and K^O are known. If either one is infinite, some spin-spin correlation does not decay to zero as $r \rightarrow \infty$, which is equivalent to the existence of *long-range order*.

3.5 Specific operators

Now we are ready to predict (in terms of K^E and K^O) the exponents η_M and η_S for the magnetization and staggered magnetization operators in the 4-state CPAFM. We shall represent the spins A, B, C, and D as unit vectors $\mathbf{m}(\mathbf{x})$ pointing toward the corners of a regular tetrahedron. The staggered magnetization $\mathbf{m}^s(\mathbf{x})$ is defined just as in Sec. 2.4. Determining the wavevectors associated with the operators $\mathbf{m}(\mathbf{x})$ and $\mathbf{m}^s(\mathbf{x})$ is trickier for the 4-state CPAFM than for the 3-state Potts AFM because of the higher dimensionality of height space. In addition, the optimal wavevector \mathbf{G} , the one giving the minimal value of $\eta_{\mathbf{G}}$, depends on the ratio K^E/K^O .

From equations (3.2) and (3.13) it is clear that the optimal \mathbf{G} may be purely even (i.e., with no component in the odd height space), purely odd, or 'mixed' (having both even and odd components), depending on whether K^E/K^O is large, small, or intermediate in value.

The minimal length reciprocal lattice vector \mathbf{G} in the purely even, purely odd, or mixed case is

$$\mathbf{G}^{\text{E}} = \left(\frac{\pi}{2}, 0, 0\right)_{\text{E}}, \quad \mathbf{G}^{\text{O}} = \left(0, \frac{\pi}{3}\right)_{\text{O}}, \quad \text{or} \quad \mathbf{G}^{\text{mix}} = \left(\frac{\pi}{4}, 0, \frac{\pi}{4}\right)_{\text{E}} + \left(0, \frac{\pi}{6}\right)_{\text{O}}, \quad (3.14)$$

respectively. Each of these is symmetry-related to other \mathbf{G} s with the same length. As it turns out, the staggered magnetization operator $\mathbf{m}^s(\mathbf{x})$ has nonzero Fourier components at \mathbf{G}^{mix} and \mathbf{G}^{E} , while the magnetization $\mathbf{m}(\mathbf{x})$ has nonzero Fourier components at \mathbf{G}^{mix} and \mathbf{G}^{O} .

Eq. (3.13) gives the corresponding exponents,

$$\eta^{\text{E}} = \frac{\pi}{8K^{\text{E}}}, \quad \eta^{\text{O}} = \frac{2\pi}{27K^{\text{O}}}, \quad \eta^{\text{mix}} = \frac{1}{2}\eta^{\text{E}} + \frac{1}{4}\eta^{\text{O}}. \quad (3.15)$$

(Since η^{E} and η^{O} are independent of the way we parameterized height space, we shall use them as surrogates for K^{E} and K^{O} in subsequent expressions.) The exponent in (3.12) is $\eta_{\min} = \min\{\eta^{\text{E}}, \eta^{\text{O}}, \eta^{\text{mix}}\}$. In particular,

$$\text{if } \eta^{\text{E}}/\eta^{\text{O}} < 1/2, \text{ then } \eta_{\min} = \eta^{\text{E}} \text{ and } \eta_{\text{M}} > \eta_{\text{S}} = \eta_{\min} = \eta^{\text{E}}, \quad (3.16\text{a})$$

$$\text{if } 1/2 \leq \eta^{\text{E}}/\eta^{\text{O}} \leq 3/2, \text{ then } \eta_{\min} = \eta^{\text{mix}} \text{ and } \eta_{\text{M}} = \eta_{\text{S}} = \eta_{\min} = \eta^{\text{mix}}, \quad (3.16\text{b})$$

$$\text{and if } \eta^{\text{E}}/\eta^{\text{O}} > 3/2, \text{ then } \eta_{\min} = \eta^{\text{O}} \text{ and } \eta_{\text{S}} > \eta_{\text{M}} = \eta_{\min} = \eta^{\text{O}}. \quad (3.16\text{c})$$

3.6 Locking exponent

Roughly speaking, there are more states with coarse-grained \mathbf{h} near a node than near an interstitial point of the ideal-states graph. In effect, an operator $f_{\text{lock}}(\mathbf{h})$ is added to the effective free energy, a periodic function of \mathbf{h} which is negative near each node of the graph. This (small) term favors ‘locking’ of the entire system into a ‘smooth’ state, which is close to one of the ideal states. It is known that locking occurs whenever the corresponding exponent η_{lock} is less than 4 (José *et al.*, 1977).

This forces our attention to the Bravais lattice of the ideal-states graph. Usually this is denser than the repeat lattice, since it includes translations which make the nodes superpose, even if they represent different ideal states. Correspondingly, \mathbf{G}_{lock} , the smallest reciprocal lattice vector of the operator f_{lock} , is typically larger than \mathbf{G}_{min} . Thus, in the 4-state CPAFM case, the ‘even’ projection of the ideal-states graph has a bcc Bravais lattice, which has twice as many points as the simple cubic repeat lattice, and correspondingly has $\mathbf{G}_{\text{lock}}^{\text{E}}$ larger than \mathbf{G}^{E} defined in Sec. 3.4. However, when the graph is considered in 5 dimensions, it turns out that its Bravais lattice is the same as the repeat lattice, since the ‘odd’ components deviate in the opposite directions from the body-corner and body-center points of the ‘even’ projection. Although the corresponding reciprocal lattice contains \mathbf{G}^{E} , there is an extinction in the Fourier transform of the ideal-states graph and thus $f_{\text{lock}}(\mathbf{h})$ does not have a component at wavevector \mathbf{G}^{E} .

We find that the optimal reciprocal lattice vector is

$$\mathbf{G}_{\text{lock}}^{\text{E}} = \left(\frac{\pi}{2}, \frac{\pi}{2}, 0 \right)_{\text{E}}, \quad \mathbf{G}_{\text{lock}}^{\text{O}} = \left(0, \frac{2\pi}{3} \right)_{\text{O}}, \quad \text{or} \quad \mathbf{G}_{\text{lock}}^{\text{mix}} = \left(\frac{\pi}{4}, \frac{\pi}{4}, 0 \right)_{\text{E}} + \left(\frac{\pi}{6}, \frac{\pi}{6} \right)_{\text{O}}. \quad (3.17)$$

(Each of these is symmetry-related to other \mathbf{G} s with the same length). Consequently, in terms of η^{E} and η^{O} as used in the preceding section,

$$\text{if } \eta^{\text{E}}/\eta^{\text{O}} < 1/6, \text{ then } \eta_{\text{lock}} = \eta_{\text{lock}}^{\text{E}} = 2\eta^{\text{E}}, \quad (3.18\text{a})$$

$$\text{if } 1/6 \leq \eta^{\text{E}}/\eta^{\text{O}} \leq 15/2, \text{ then } \eta_{\text{lock}} = \eta_{\text{lock}}^{\text{mix}} = \frac{1}{4}\eta_{\text{lock}}^{\text{E}} + \frac{1}{16}\eta_{\text{lock}}^{\text{O}}, \quad (3.18\text{b})$$

$$\text{and if } \eta^{\text{E}}/\eta^{\text{O}} > 15/2, \text{ then } \eta_{\text{lock}} = \eta_{\text{lock}}^{\text{O}} = 4\eta^{\text{O}}. \quad (3.18\text{c})$$

4 Monte Carlo simulation

To obtain more information on the 4-state CPAFM we performed a Monte Carlo simulation of the model. By averaging appropriate quantities over the ensemble of allowed states, we can independently determine the stiffnesses, K^E and K^O , and any correlation exponents. The results can then be examined in light of Section 3.

Although we are only particularly interested in the case $q = 4$, we developed an algorithm for simulating the general q -state CPAFM. This permitted us to perform a partial check of our code by simulating the $q = 3$ Potts AFM and comparing our Monte Carlo results with the known exact results for that model.

4.1 Monte Carlo algorithm

We chose to use periodic boundary conditions in the simulation. Given this choice, it is natural to require that the number of rows and columns in the lattice both be even numbers; otherwise, there can be no well-defined even and odd sublattices and, hence, the odd heights are not well-defined. In addition, there would be no allowed configuration corresponding to a single ideal state.

4.1.1 Initial state

We performed runs with each of three types of initial state. The simplest choice is one of the $2q$ ideal states. All the spins in one sublattice are set to the same value, while the spins in the other, disordered sublattice are chosen randomly from the remaining $q - 1$ possible values. The most important property of this state is that it is ‘flat’ in height space (the coarse-grained height is constant throughout the system). As the system evolves into a rough state, the Fourier spectrum $\langle |\mathbf{h}(\mathbf{q})|^2 \rangle$ increases from zero to the equilibrium value, for most \mathbf{q} .

A second, more elaborate method is to divide the lattice into an array of smaller blocks; each block is assigned a random ideal state (to be filled in as described above), with certain

restrictions to ensure that only allowed configurations are obtained for the full lattice. This initial state is also macroscopically flat.

A third, contrasting kind of initial state for a height model is not macroscopically flat; it has, locally, the maximum possible height-space slope (Kondev and Henley, 1995a; Kondev and Henley, 1995b; Raghavan *et al.*, 1997). It is called a ‘roof’ configuration since it is usually composed of two domains of opposite slope. (The system-average slope must be zero in order for the states of lowest free energy to be accessible by local updates.) The ‘roof’ configuration shown in Figure 4 includes 4 domains of periodic states. In each domain (considered as a state in the $q = 4$ model), the odd heights are flat, while the even heights vary as rapidly as allowed. In this case, many Fourier amplitudes are large at first and approach their equilibrium values from above. Thus, by iterating until the expectation value is independent of initial configuration, we can ensure that equilibrium is reached.

4.1.2 Update move

An update move must satisfy three conditions:

- (i) it must change any allowed configuration into another allowed configuration;
- (ii) it must be ergodic – i.e., through a sequence of update moves, any allowed configuration must be accessible from any other one; and
- (iii) it must satisfy detailed balance.

In the CPAFM model the first condition is nontrivial: a single spin-flip is disallowed on many sites because of the nearest-neighbor and plaquette constraints, and the remaining allowed single-spin flips are too few to be ergodic. Thus a cluster-update move is a *necessity* for the CPAFM ground-state ensemble.⁷ Clearly, within a cluster, the change should be a global symmetry of the model, i.e. an exchange of Potts states X and Y . (An allowed single-spin flip is a special case of this.)

⁷In the 3-state Potts AFM, it is an optional improvement to obtain acceleration (Wang *et al.*, 1990).

The update move we used is to

- (1) Pick a site \mathbf{x} at random; say $\sigma(\mathbf{x}) = X$, and randomly choose $Y (\neq X)$ to be any of the $q - 1$ values of spin.
- (2) Determine the minimal domain containing site \mathbf{x} in which it is allowable to exchange $X \leftrightarrow Y$ on all sites (we call this the ‘ XY -cluster’ of site \mathbf{x}), and do so.

The geometrical rules for an XY -cluster are simple. We define a link (in the percolation sense) between sites \mathbf{x} and \mathbf{x}' if either (i) they are nearest neighbors and have spin values X and Y ; or (ii) they are second-neighbors, both with spin X or both with spin Y , and the other two spins on the plaquette are different. Then the XY -cluster consists of all sites connected to \mathbf{x} by such links; in this fashion all X and Y spins are divided into disjoint clusters, as in a percolation model. Clearly, performing $X \leftrightarrow Y$ on one endpoint of a link and not the other creates a disallowed state, so we must at least update the XY -cluster; it is easy to see that it is also sufficient to do so.

Since the exchange $X \leftrightarrow Y$ does not change the pattern of XY -clusters, the update move is reversible: it can change configuration Φ directly into configuration Ψ if and only if it can change Ψ directly into Φ . Furthermore, the probability of flipping a given XY -cluster in an update step is just $1/(q-1)$ times the fraction of all lattice sites which belong to that cluster (since we would have flipped the same cluster if we had initially hit on any of its sites and chosen the appropriate second spin value). Hence the rate of $\Phi \rightarrow \Psi$, given configuration Φ , is the same as the rate $\Psi \rightarrow \Phi$, given Ψ ; for our ensemble, in which all allowed configurations have equal weight, this is the detailed balance property. The only thing left is to verify the ergodicity of the update move, which is done in Appendix C.

In speaking of ergodicity, we should make clear that, in the presence of periodic boundary conditions, any *local* update move conserves the net height difference (tilt) across the system and hence is non-ergodic in a trivial sense. However, our cluster update move is *nonlocal* and can change the net tilt.

It is interesting to note that, in terms of the height variables $\mathbf{z}(\mathbf{x})$, the update move simply inverts the even height components on the sites within the updated cluster (the cluster boundary is a loop of constant height, as studied by Kondev and Henley (1995a), so the height is unchanged along it). This reflection is closely related to the ‘valleys-to-mountains reflection’ algorithm (Evertz *et al.* , 1991; Hasenbusch *et al.* , 1992). On the other hand, the odd height components on the cluster sites are simply shifted by a constant vector.

4.2 Measurements

Simulation runs were performed for lattices of various sizes ranging from 16×16 to 200×200 . As mentioned above, since the notion of even and odd sublattices is essential in these models, the number of sites in a row or column of the lattice was always chosen to be even. In runs where Fourier transforms were taken, fast Fourier transform (FFT) algorithms were used and, hence, it was also convenient in these runs to have the number of sites in a row or column be a power of two.

Since successive states are highly correlated, any measurements were taken once per sampling interval; the duration of a sampling interval (as a number of cluster hits) was varied depending on the lattice size. Furthermore, in order to estimate uncertainties in the calculated averages, we computed averages and variances using groups of 100 sampling intervals. Averages over successive groups were treated as uncorrelated for the purpose of estimating uncertainties.

We made the following measurements. At each sampling time, the height configuration $\mathbf{z}(\mathbf{x})$ was generated from the spin configuration. Then $\mathbf{h}(\mathbf{q})$, the Fourier transform of the height configuration $\mathbf{z}(\mathbf{x})$, was computed (via FFT). The average of $|\mathbf{h}(\mathbf{q})|^2$ was accumulated for every wavevector \mathbf{q} .

We must note that our procedure in generating $\mathbf{z}(\mathbf{x})$ is not quite safe. The FFT requires that $\mathbf{z}(\mathbf{x})$ obey periodic boundary conditions; but if the configuration has a net tilt in height

space, the algorithm leaves a ‘seam’ along the edges of the lattice, across which $\mathbf{z}(\mathbf{x})$ has a sudden jump. (Recall that the tilt can be changed by the algorithm only in the rare event than an update XY -cluster winds nontrivially around the periodic boundaries.) If ‘tilted’ configurations are frequent, this causes a spurious contribution to $\langle |\mathbf{h}(\mathbf{q})|^2 \rangle$ for (only) \mathbf{q} lying on the x and y axes of Fourier space.⁸ That would be visible in data plots such as Figure 6: those data points would form a separate curve, shifted above the points from elsewhere in Fourier space. In fact, the plotted points appear to fall along a single curve. Therefore we believe that configurations with height-space tilt are rare and do not affect our results. (If the system is in a ‘smooth’ phase, as discussed in Sec. 5, suppression of tilt is just what one would expect.)

For the 4-state model, additional measurements were made. We computed the total magnetization $\mathbf{M} = \sum \mathbf{m}(\mathbf{x})$ and staggered magnetization $\mathbf{M}^s = \sum \mathbf{m}^s(\mathbf{x})$, and accumulated averages of $|\mathbf{M}|^2$ and $|\mathbf{M}^s|^2$. Also, we measured the size distribution of the XY -clusters.

⁸Such behavior was very obvious in (unpublished) test runs of Kondev and Henley (1995b). Their published data were from simulations that disallowed any update moves that would have changed the tilt.

5 Simulation results and discussion

We will now present and discuss the Monte Carlo data. Our chief interest is whether the heights are in a smooth or a rough phase, corresponding respectively to long-range order or power-law correlations of the underlying Potts spins. Since the ‘even’ and ‘odd’ height components are not related by symmetry, it is also possible that one kind could be smooth and the other kind could be rough, as occurs in the dimer-loop model (Raghavan *et al.* , 1997).

The ‘smooth’ scenario is favored by measurements of the height fluctuations, which contain the most information (Secs. 5.1 and 5.2). On the other hand, direct measurements (Sec. 5.3) of the order parameters suggest a ‘rough’ phase. The evidence will be judged in Sec. 5.4.

As a test, we simulated the 3-state Potts AFM (using the same code, as explained in Sec. 4), so as to compare with exact results. (The 3-state model, in its representation as the BCSOS model, was also used for test simulations by Raghavan *et al.* (1997).) According to the theory in Sec. 2, $\lim_{q \rightarrow 0} |\mathbf{q}|^2 \langle |h(\mathbf{q})|^2 \rangle = 1/K$. In Figure 5 we show $|\mathbf{q}|^2 \langle |h(\mathbf{q})|^2 \rangle$ vs. $|\mathbf{q}|^2$ for the 3-state simulation on a 64×64 lattice. Clearly this quantity does approach a constant as $|\mathbf{q}| \rightarrow 0$. Although the statistical uncertainty in each data point is $\approx 10\%$, the uncertainty of the intercept in Figure 5 is only $\approx 1\%$ according to a least squares fit. The fitted inverse stiffness constant is $1/K = 1.92 \pm 0.02$, which is in excellent agreement with the known exact value of $6/\pi \approx 1.91$.

5.1 Fourier mode fluctuations

The expected behavior of the height components, in the limit $q \rightarrow 0$ and $L \rightarrow \infty$, can be put in the form

$$\langle |\tilde{h}_i(\mathbf{q})|^2 \rangle \sim \frac{C_i}{q^{2-y_i}}. \quad (5.1)$$

When the height components are rough and described by a gradient-squared free energy, Eq. 3.3, then $y_i = 0$ and $C_i = (\mathbf{K}^{-1})_{ii}$. If we define height components to be ‘smooth’ either when $(\mathbf{K}^{-1})_{ii} = 0$, or when the height fluctuations are bounded independent of system size, this is equivalent to $y_i > 0$ in (5.1). In such a case, the boundedness of height fluctuations, $\langle |\mathbf{h} - \mathbf{h}'|^2 \rangle < \text{const}$, implies, when inserted in (2.13), that operator correlations $\langle O(\mathbf{x})O(\mathbf{x}') \rangle$ are bounded below as $|\mathbf{x} - \mathbf{x}'| \rightarrow \infty$. One’s usual picture of a ‘smooth’ phase is a background of long-range order, on which some height fluctuations with rapidly decaying correlations are superposed. That would imply q -independent behavior of (5.1) at long wavelengths, i.e. $y = 2$.

Figure 6 shows $\log(q^2 \langle |h_1(\mathbf{q})|^2 \rangle)$ vs. $\log(q^2)$ for the 4-state simulation on a 64×64 lattice. The slope of the graph at small q is $y_1/2$ and its evident nonzero value implies that h_1 is smooth. A linear fit to the small- q data gave

$$y_1 = 0.27 \pm 0.02, \quad (5.2)$$

where the uncertainty reflects the dependence on choosing an upper cut-off q for data points to be used in the fit. The data for h_2 and h_3 (not shown) indicate similar values for y_2 and y_3 , as expected from the symmetry among all even height components.

As for the ‘odd’ height components, we find numerically for all $\mathbf{q} (\neq 0)$ that

$$\langle |\mathbf{h}_{\text{odd}}(\mathbf{q})|^2 \rangle = 3 \langle |\mathbf{h}_{\text{even}}(\mathbf{q})|^2 \rangle. \quad (5.3)$$

This is seen in the nice overlap of plots of $q^2 \langle |h_1(\mathbf{q})|^2 \rangle$ and $q^2 \langle |h_4(\mathbf{q})|^2 \rangle / 3$ against q^2 (Figure 7). The corollary of (5.3) is that y_i has the same value for all height components. (The significance of (5.3) is discussed in Sec. 5.2.) Hence all height components are ‘smooth’ and we expect the spins to exhibit long-range order.

However, as noted above, the expectation for a smooth phase would be $y_i = 2$, contrary to (5.2). Therefore, we carried out a finite size analysis to check whether the low- q behavior was a system-size effect. For nonzero q and finite L we expect (5.1) to generalize to

$$\langle |\tilde{h}_i(\mathbf{q})|^2 \rangle = q^{y_i-2} f_i(q, L), \quad (5.4)$$

where $f_i(q, L)$ is a scaling function that approaches C_i as $q \rightarrow 0$ and $L \rightarrow \infty$. Figure 8 shows a plot of $q^2 \langle |h_1(\mathbf{q})|^2 \rangle$ vs. q^2 for 16×16 , 32×32 , and 64×64 lattices. The nice overlap of the three functions indicates that L in these runs is sufficiently large that $f_i(q, L)$ is a function of q only.

The finite size of L also imposes a limit on the smallest nonzero wavevectors \mathbf{q} which can be probed in a simulation. But the plot in Figure 6 appears rather linear (as already noted, its slope varies by only ± 0.02 over a large range of q values), which would suggest that the q values accessible in the $L = 64$ simulation are small enough that $f_i(q, L)$ is close to $f_i(0, L)$, and hence that the value extracted for y_i in (5.2) is close to the correct asymptotic one.

5.2 Ratio of ‘even’ and ‘odd’ height fluctuations

The ratio of 3 in Eq. (5.3) is nontrivial. It is certainly not true that $|\mathbf{h}_{\text{odd}}(\mathbf{q})|^2 = 3|\mathbf{h}_{\text{even}}(\mathbf{q})|^2$ for every allowed configuration; indeed, Figure 4 shows a case where $|\mathbf{h}_{\text{odd}}(\mathbf{q})|^2$ is (essentially) zero while $|\mathbf{h}_{\text{even}}(\mathbf{q})|^2$ is unusually large for $\mathbf{q} = (0, \pm\pi/L)$ or $(\pm\pi/L, 0)$. Nor could we find any hidden symmetry relating the ‘even’ and ‘odd’ height components.

There is a simple explanation for the observation (5.3) if we postulate that

- (i) both even and odd height components are ‘smooth’, and
- (ii) the system is dominated by domains of a single ideal state, with small independent domains of the three other ideal states which are most similar to it.

In the ideal-states graph, those neighboring ideal states have vertices surrounding that of the dominant state, forming 120° angles. (The same angles may be seen in both the even and odd projections of the ideal-states graph.) Consequently the height fluctuations all occur in a rank-2 subspace of height space and in particular, $\mathbf{h}_{\text{even}}(\mathbf{q})$ is a linear multiple of $\mathbf{h}_{\text{odd}}(\mathbf{q})$. The linear ratio is in fact $1/\sqrt{3}$ – the ratio of the even and odd components in Table 1 – and (5.3) follows immediately.

In fact, if the fluctuations occurred around a single ideal state, there would be cross-correlations between $\mathbf{h}_{\text{even}}(\mathbf{q})$ and $\mathbf{h}_{\text{odd}}(\mathbf{q})$. However, thanks to the cluster update move, the

dominant domain is frequently being changed; thus cross-correlations are averaged to zero.

In fact, we can even extend this argument to permit domains which are *two* steps away from ‘AX’ on the ideal-states graph. The second neighbor distances on the ideal-states graph are also in the ratio $1/\sqrt{3}$, so that the contributions of *any single domain* to $\mathbf{h}_{\text{even}}(\mathbf{q})$ and $\mathbf{h}_{\text{odd}}(\mathbf{q})$ are still in the right ratio. However, the different domains do span a space of rank greater than 2, so the total $\mathbf{h}_{\text{even}}(\mathbf{q})$ and $\mathbf{h}_{\text{odd}}(\mathbf{q})$ are no longer linear multiples. Nevertheless, if the locations of the different domains are statistically independent, then cross-terms between different domains must cancel and one again obtains (5.3). Because small inter-domain correlations must exist, and there must be rare domains which are three steps away from the dominant one (third neighbor distances on the ideal-states graph are not in the right ratio), we conjecture that, in fact, there are tiny deviations from an exact ratio of 3 in (5.3).

Thus, the observed ratio of 3 implies bounded fluctuations, which imply long-range order. Indeed, the only way we expect this behavior is when a finite fraction of the allowed configurations contain an AX domain that occupies a finite fraction of the lattice.

5.3 System-size scaling of operators

Say an operator $O(\mathbf{x})$ has correlations $\langle O(\mathbf{x})O(\mathbf{x}') \rangle \sim r^{-\eta}$, and the corresponding order parameter is defined as $M_O = \sum_{\mathbf{x}} O(\mathbf{x})$. Then simply expanding the double sum in $\langle M_O M_O \rangle$ for a system of $N = L^2$ sites gives

$$\langle |M_O|^2 \rangle \sim L^{4-\eta} \sim N^{2-\eta/2}. \quad (5.5)$$

In particular, $\langle |M_O|^2 \rangle \sim N^2$ in a system with long-range order. We measured expectation (5.5) for $M_O \rightarrow \mathbf{M}$ and $M_O \rightarrow \mathbf{M}^s$, corresponding to exponents η_M and η_S defined in Sec. 3.5.

Figure 9 shows a log-log plot of $\langle |\mathbf{M}|^2 \rangle$ from the 4-state simulations with three system sizes N . The data points fit to a line with slope 1.85 ± 0.01 (fitting error only!), i.e.

$$\langle |\mathbf{M}|^2 \rangle \sim N^{1.85} \quad (5.6)$$

for N in the range simulated.

We also measured the average total staggered magnetization for lattices of size 64×64 and 120×120 ; connecting these two data points would imply

$$\langle |\mathbf{M}^s|^2 \rangle \sim N^{1.93}. \quad (5.7)$$

Eqs. (5.6) and (5.7) respectively imply

$$\eta_M \approx 0.30 \pm 0.02, \quad \eta_S \approx 0.14. \quad (5.8)$$

5.4 Discussion: rough or smooth?

The magnetization behavior reported in Sec. 5.3 is that expected for rough heights and critical spin correlations, which is in contradiction to our conclusion from Fourier fluctuations in Sec. 5.1. Which inference should we believe? We shall attempt to make sense of the data assuming a ‘rough’ state, and show it leads to several contradictions.

We start with the $\mathbf{h}(\mathbf{q})$ data. The ratio of 3 in (5.3), which is our surest and most precise numerical result, implies that $K^O = \frac{4}{9}K^E$. Then, in the notation of Sec. 3.5, it would follow that

$$\eta^E = \frac{\pi}{8K^E}, \quad \eta^O = \frac{\pi}{6K^E}, \quad \eta^{\text{mix}} = \frac{5\pi}{48K^E}, \quad (5.9)$$

and hence

$$\eta_M = \eta_S = \eta^{\text{mix}}. \quad (5.10)$$

Roughness means that the curve in Figure 6 asymptotes to a constant as $q \rightarrow 0$; we may assume it does so monotonically, so the smallest visible value provides a lower bound on the stiffnesses, $K^E \geq 1.5$, i.e.

$$\eta^{\text{mix}} \leq 0.22. \quad (5.11)$$

The conclusion $\eta_M = \eta_S$ in Eq. (5.10) is incompatible with the unequal values obtained in Eq. (5.8); furthermore, the value $\eta_M \approx 0.30$ found from the magnetization data violates the inequality (5.11).

Most convincingly, since $\eta^E/\eta^O = 3/4$ we find (from (3.15) and (3.18b)) that the locking exponent of Sec. 3.6 is $\eta_{\text{lock}} = \eta_{\text{lock}}^{\text{mix}} \leq 0.2$, far smaller than the critical value 4. Then (José *et al.*, 1977) the effective stiffness constant becomes larger and larger on longer length scales, so the system must lock into a ‘smooth’ phase. So, based on all the above arguments, we conclude that the system must be in a ‘smooth’ phase.

We can check this picture by examining the system in real space. Long-range order, in which the system locks into a particular ideal state, means that a typical configuration should look like an ideal state with some disorder: that is, there should be an excess of one particular spin label on one sublattice and a paucity of that spin label on the other sublattice, even in an infinite lattice.

A measurement of this tendency can be gleaned from our results on the size distribution of *XY*-clusters (these were defined in Sec. 4.1.2). A substantial fraction of the encountered configurations had an *XY*-cluster which included more than half of all sites; the frequency of such configurations decreases with lattice size, but is still quite appreciable at our largest lattice size, 200×200 . Thus we cannot decide whether or not the frequency is zero in the thermodynamic limit.

To further illustrate the tendency to long-range order, Figure 10 shows a typical configuration (after equilibration) in the 4-state simulation. Note that roughly 2/3 of the sites in one sublattice have spin A whereas less than 3% of the sites in the other sublattice have spin A. In addition, all of the spin A sites in the ordered sublattice have the same height. The remaining sites are divided roughly equally among the remaining spin labels B, C, and D. These are the correlations expected in a long-range-ordered ‘AX’ type state. The fluctuations from the ‘AX’ state (where the first sublattice has a spin other than A) appear to be domains of other ideal states that are one step from ‘AX’ on the ideal states graph; that is consistent with our explanation of the ratio of 3 in Sec 5.2.

A final check of the long-range order hypothesis is to compute the total variance of each height component around its mean, which is $\langle |z_i(\mathbf{x})|^2 \rangle = \frac{1}{N} \sum_{\mathbf{q} \neq 0} \langle |h_i(\mathbf{q})|^2 \rangle$. This comes out

to be about 0.6 for the ‘even’ heights, which is also consistent with the picture just presented.

As a tentative resolution of the contradictory features of our data, we suggest that our model may be close to, or even at, the unlocking (=roughening) transition. In that case the correlation length would be very large and it would be hopeless to detect the asymptotic behavior of the staggered magnetization in accessible system sizes. (We believe that the data in Figure 9 are not indicative of the asymptotic behavior as $N \rightarrow \infty$.)

The anomalous power $y = 0.27$ extracted from the height fluctuation data might be explained if the proper functional form were

$$\langle |\mathbf{h}(\mathbf{q})|^2 \rangle \sim \log |q_0/q|/|\mathbf{q}|^2. \quad (5.12)$$

This functional form is close to that for the ‘rough’ case, but strictly speaking the behavior would be ‘smooth’. If we define an effective exponent $y_{\text{eff}} = 2 - d \log (\langle |\mathbf{h}(\mathbf{q})|^2 \rangle) / d \log q$, then taking q_0 to be the width of the Brillouin zone, we obtain $y_{\text{eff}} = 1 / \log (q/q_0) \approx 1 / \log(64) = 0.24$, which is comparable to the measured value.

6 Conclusions

We have found a spin model which has a height representation but still has long-range order in the ground state. It proved infeasible to detect the long-range order through studying fluctuations in the magnetization because the necessary system size is too large. However, by observing instead the fluctuations in the Fourier transformed height, we find conclusive evidence for long-range order through simulating systems of reasonable size.

To discuss the possible finite-temperature behavior of this model, and its relation to other models, let us display a Hamiltonian which has the CPAFM as its (degenerate) ground states:

$$H = -\frac{1}{2} \sum_{\text{n.n. } \mathbf{x}, \mathbf{x}'} J_1 \delta_{\sigma(\mathbf{x}), \sigma(\mathbf{x}')} - \frac{1}{2} \sum_{\text{n.n.n. } \mathbf{x}, \mathbf{x}''} J_2 \delta_{\sigma(\mathbf{x}), \sigma(\mathbf{x}'')} - \sum_{\text{plaq. } \mathbf{x}, \mathbf{x}', \mathbf{x}'', \mathbf{x}'''} J_4 \delta_{\sigma(\mathbf{x}), \sigma(\mathbf{x}'')} \delta_{\sigma(\mathbf{x}'), \sigma(\mathbf{x}''')}, \quad (6.1)$$

where the second sum is taken over second nearest neighbors, and the last sum is over plaquettes with $\mathbf{x}, \mathbf{x}', \mathbf{x}'', \mathbf{x}'''$ in cyclic order around the plaquette. We must take the case $J_4 = -J_2$, making the plaquettes of type (ABAB) and (ABCB) degenerate, to make the CPAFM states all degenerate and justify their equal weights.

At $T > 0$, typical configurations violate the CPAFM constraint at rare places; this creates dislocation defects in the height field; when $\mathbf{h}(\mathbf{x})$ is followed along a closed loop around that defect it is shifted by a height-space Burgers vector \mathbf{b} (which is in the repeat lattice). The correlations of these defects are described by vortex-vortex (i.e. ‘magnetic’) type exponents in the Coulomb-gas picture (Nelson, 1983; Nienhuis, 1987). It can be shown that the specific heat and inverse correlation length behave as $e^{-cE_0/T}$, where E_0 is the energy cost of a defect, and the coefficient c is related to its Burgers vector and the stiffness constant(s) (Huse and Rutenberg, 1992; Read, 1992; Kondev and Henley, 1995a; Kondev and Henley, 1995b; Kondev and Henley, 1996).⁹

The best-known height models with critical ground states, in particular the 3-state Potts

⁹This confirms that when Wang *et al.* (1989; 1990) fitted the specific heat of the 3-state Potts AFM to the form e^{C/T^x} , they should have obtained $x = 1$ (Ferreira and Sokal, 1995).

AFM, have stiffness constants K such that the defects are unbound, i.e., the system is in the same phase as the two-dimensional XY -ferromagnet above its Kosterlitz-Thouless transition temperature. In such a case, $T = 0$ is a critical point with the spin model being disordered at any finite temperature, since that means that the fugacity of the height defects, $e^{-E_0/T}$, is nonzero. A richer behavior is shown by the large- S triangular Ising antiferromagnet: the height field ensemble for the ground state is ‘smooth’ (i.e. the ground state has long-range order), and then as T is increased there are two transitions at finite T , first to a critical state and then to a disordered one (Lipowski *et al.*, 1995). Since we find that the CPAFM model is ‘smooth’ at $T = 0$, it seems quite plausible that it undergoes analogous transitions at $T > 0$.

The Hamiltonian (6.1) is equivalent to a Boltzmann weight (for each possible configuration of Potts spins)

$$W = \prod_{\text{n.n. } \mathbf{x}, \mathbf{x}'} (1 - x \delta_{\sigma(\mathbf{x}), \sigma(\mathbf{x}')}) \times \prod_{\text{plaq. } \mathbf{x}, \mathbf{x}', \mathbf{x}'', \mathbf{x}'''} [u + v (\delta_{\sigma(\mathbf{x}), \sigma(\mathbf{x}'')} + \delta_{\sigma(\mathbf{x}'), \sigma(\mathbf{x}''')}) + y \delta_{\sigma(\mathbf{x}), \sigma(\mathbf{x}'')} \delta_{\sigma(\mathbf{x}'), \sigma(\mathbf{x}''')}] . \quad (6.2)$$

The CPAFM constraints correspond to $x \equiv 1$ and $u \equiv 0$ in (6.2); the equal-weighted ensemble means also taking $v = -y > 0$. Nienhuis (1990) studied the case where $y \equiv 0$ (see his Eq. (3)), which is a different weighting of the same constrained states. By mapping it to a loop model, he investigated this model with the number of Potts states q as a continuous variable. It was found (see his Eq. (12)) that the model is critical when $q \leq q_c = 3$ (but would have long-range order when $q > q_c$). Our Boltzmann weighting, with $y < 0$, disfavors the very flat ‘ABAB’ type plaquettes (relative to Nienhuis’s weighting) and thus should be rougher, with $q_c \geq 3$ in our case; this is all consistent with our conclusion that the model is smooth, but possibly is near the roughening transition.

In Sec. 5, we speculated that the CPAFM model might be near the unlocking (roughening) transition. The 3-state Potts AFM on the Kagomé lattice (Huse and Rutenberg, 1992) and the edge 4-coloring of the square lattice (Kondev and Henley, 1995a; Kondev and Henley,

1995b; Kondev and Henley, 1996) are known, in the ensemble where all configurations are weighted equally, to be exactly at their roughening transitions, i.e. the locking operator is marginal. In the latter case $\langle |\mathbf{h}(\mathbf{q})|^2 \rangle$, as measured in Monte Carlo simulations (Kondev and Henley, 1995b), shows a clean $1/|\mathbf{q}|^2$ behavior just like a non-marginal rough case. In the dimer-loop model (Raghavan *et al.*, 1997), one of the two height components shows clean $1/|\mathbf{q}|^2$ behavior indicating roughness, but the other component shows an intermediate power somewhat like our findings for the CPAFM model.

Acknowledgements:

We would like to thank J. Kondev, B. Nienhuis, R. Raghavan, and C. Zeng for discussions and comments. This work was supported by NSF grant No. DMR-9214943.

References

- Banavar, J. R., Grest, G. S., and Jasnow, D. (1980). *Phys. Rev. Lett.* **45**, 1424.
- Baxter, R. J. (1970). *J. Math. Phys.* **11**, 3166.
- Blöte, H. W. J., and Hilhorst, H. J. (1982). *J. Phys. A* **15**, L631.
- Coxeter, H. S. M. (1955). *Can. J. Math.* **7**, 18.
- den Nijs, M., Nightingale, M. P., and Schick, M. (1982). *Phys. Rev. B* **26**, 2490.
- Evertz, H. G., Hasenbuch, M., Marcu, M., Pinn, K., and Solomon, S. (1991). *Phys. Lett. B* **254**, 185.
- Ferreira, S. J., and Sokal, A. D. (1995). *Phys. Rev. B* **51**, 6727.
- Fisher, M. E., and Stephenson, J. (1963). *Phys. Rev.* **132**, 1411.
- Gottlob, A. P., and Hasenbusch, M. (1994). *J. Stat. Phys.* **77**, 919.
- Grest, G. S., and Banavar, J. R. (1981). *Phys. Rev. Lett.* **46**, 1458.
- Hasenbusch, M., Lana, G., Marcu, M., and Pinn, K. (1992). *Phys. Rev. B* **46**, 10472.
- Huse, D. A., and Rutenberg, A. D. (1992). *Phys. Rev. B* **45**, 7536.
- José, J. V., Kadanoff, L. P., KirkPatrick, S. R., and Nelson, D. R. (1977). *Phys. Rev. B* **16**, 1217.
- Kolafa, J. (1984). *J. Phys. A* **17**, L777.
- Kolesik, M., and Suzuki, M. (1995). *J. Phys. A* **28**, 1543.
- Kondev, J., and Henley, C. L. (1995a). *Phys. Rev. Lett.* **74**, 4580.
- Kondev, J., and Henley, C. L. (1995b). *Phys. Rev. B* **52**, 6628.

- Kondev, J., and Henley, C. L. (1996). *Nuc. Phys. B* **464**, 540.
- Leu, J. A., Betts, D. D., and Elliott, C. J. (1969). *Can. J. Phys.* **47**, 1671.
- Levitov, L. S. (1990). *Phys. Rev. Lett.* **64**, 92.
- Lieb, E. H., and Wu, F. Y. (1972). In *Phase Transitions and Critical Phenomena* (ed. C. Domb and M. S. Green), Vol. I. Academic, London.
- Lipowski, A., Horiguchi, T., and Lipowska, D. (1995). *Phys. Rev. Lett.* **74**, 3888.
- Lubin, M., and Sokal, A. D. (1993). *Phys. Rev. Lett.* **71**, 1778.
- Nelson, D. R. (1983). In *Phase Transitions and Critical Phenomena* (ed. C. Domb and J. L. Lebowitz), Vol. 7. Academic, London.
- Nienhuis, B. (1987). In *Phase Transitions and Critical Phenomena* (ed. C. Domb and J. L. Lebowitz), Vol. 11. Academic, London.
- Nienhuis, B. (1990). *Int. J. Mod. Phys.* **4**, 929.
- Nienhuis, B., Hilhorst, H. J., and Blöte, H. W. J. (1984). *J. Phys. A* **17**, 3559.
- Park, H., and Widom, M. (1989). *Phys. Rev. Lett.* **63**, 1193.
- Raghavan, R., Henley, C. L., and Arouh, S. L. (1997). *J. Stat. Phys.* **86**, 517.
- Read, N. (1992). In *Proceedings of Kagomé workshop* (ed. P. Chandra). NEC Laboratories, NJ, USA.
- van Beijeren, H. (1977). *Phys. Rev. Lett.* **38**, 993.
- Wang, J-S., Swendsen, R. H., and Kotecký, R. (1989). *Phys. Rev. Lett.* **63**, 109.
- Wang, J-S., Swendsen, R. H., and Kotecký, R. (1990). *Phys. Rev. B* **42**, 2465.
- Wannier, G. H. (1950). *Phys. Rev.* **79**, 357.

Zeng, C., and Henley, C. L. (1997). *Phys. Rev. B* **55**, 14935.

Zheng, W., and Sachdev, S. (1989). *Phys. Rev. B* **40**, 2704.

APPENDIX A: Dimensionality of height space

In this Appendix we show that the height space has dimension 5 as asserted in Sec. 3.1. To do this, we first construct the most general mapping of a configuration to a height-like vector, such that the height steps between two sites depends only on their respective spin values σ , σ' and on the parity ϵ of (say) the first site.¹⁰ This turns out to give 12 candidate height components. Then we show that only five of these are valid, nontrivial height components, and finally we show (by examples) that no further reduction of the dimensionality is possible.

Note first that $\Delta\mathbf{z}(\sigma, \sigma', \epsilon) \equiv -\Delta\mathbf{z}(\sigma', \sigma, -\epsilon)$ since the left- and right-hand sides are the height difference of the steps from \mathbf{x} to \mathbf{x}' and back again; thus, it suffices to define $\Delta\mathbf{z}$ for $\epsilon = +1$. There are $q(q-1) = 12$ possible combinations of (σ, σ') since neighbors cannot have the same spin value; thus all possible functions form a 12-dimensional linear space, labeled by $(X, Y) \in \{A, B, C, D\}^2$ with $X \neq Y$.

A candidate height component $\zeta_{XY}(\mathbf{x})$ is defined so $\Delta\zeta_{XY} = +1$ if $(\sigma, \sigma', \epsilon) = (X, Y, +1)$, $\Delta\zeta_{XY} = -1$ if $(\sigma, \sigma', \epsilon) = (Y, X, -1)$, and zero otherwise. In the CPAFM model, it can be checked that every component ζ_{XY} is well-defined, by encircling each plaquette. (If we encounter an XY step, we must also encounter a YX step, e.g. in the plaquette $XYXZ$.)

A.1 Reduction to nontrivial height components

Some linear combinations of the components $\zeta_{XY}(\mathbf{x})$ are bounded so the corresponding subspaces of the 12-dimensional candidate height space are trivial. Namely, let $\rho_{\sigma,E}(\mathbf{x}) = +1$ when \mathbf{x} is an even site and its spin takes the value σ , and let $\rho_{\sigma,E}(\mathbf{x}) = 0$ otherwise; let $\rho_{\sigma,O}(\mathbf{x})$ be the analogous function for odd sites. Then $\rho_{\sigma,E}(\mathbf{x}) = -\sum_{\sigma' \neq \sigma} \zeta_{\sigma\sigma'}(\mathbf{x})$ (modulo a global additive constant), as can be checked by inspection of the possible $\Delta\rho_{\sigma,E}$ values; similarly $\rho_{\sigma,O}(\mathbf{x}) = +\sum_{\sigma' \neq \sigma} \zeta_{\sigma'\sigma}(\mathbf{x})$ (modulo a constant). There is one linear dependence among the $2q = 8$ distinct ρ functions, since $\sum_{\sigma} (\rho_{\sigma,E}(\mathbf{x}) + \rho_{\sigma,O}(\mathbf{x})) = 1$. Thus there is

¹⁰This assumption is justified since the height rule ought always to have the same lattice periodicity as an ideal state, which is a two-sublattice pattern for the CPAFM case.

a seven-dimensional trivial subspace of ζ space; the remaining five dimensions, it can be checked, are spanned by the five height components defined in Sec. 3.1. (For the q -state CPAFM model, this construction would give $q^2 - 3q + 1$ dimensions.)

A.2 Necessity of all five components

It remains to be shown that there is no further reduction of the height space dimensionality – that all five components are necessary. The easiest way to exclude the existence of a zero (or bounded and hence trivial) linear combination is by counterexample: we just exhibit five configurations, each of which has a net gradient only of the corresponding height component. We need only consider a one dimensional gradient.

The bottom half of Table 2 shows the height steps corresponding to a four spin sequence like $(ABCD)$ (assumed followed by another A). Consider now the 10-spin sequence $(ACBD)(ABC)(ACBD)(ACB)$. If the first $(ACBD)$ subsequence starts on an even site, then the second $(ACBD)$ starts on an odd site; hence the even components of the steps are both $(4, 0, 0)_E$ but the odd components cancel. Also, the height step of (ABC) (beginning on an even site) is canceled (in every component) by the height step of (ACB) (beginning on an odd site). Thus the net height step is $(8, 0, 0)_E$. A configuration, consisting of repeats of the 10-spin sequence, has a gradient of only the first even height component. By use of $(ABCD)$ and $(ACDB)$, we can construct a string of spins with a gradient of only the second or third even components.

Furthermore, we could reverse the second copy of the 4-spin subsequence, obtaining (say) $(ACBD)(ABC)(ADBC)(ACB)$. This reverses the height step of the second 4-spin subsequence, so that now the even components cancel and the odd components add up. In this fashion we can construct a string which has a gradient of only the first or second *odd* height component. Thus, the five height components used in this paper are nontrivial.

It should be noted that the above statement concerns only the allowed microstates of the system. It is possible – and indeed, likely in models with many height components – that

some of the components are “smooth”. That is, although they *can* have arbitrarily large fluctuations (in an arbitrarily large system), the actual fluctuations are essentially bounded due to collective effects. Thus, it may be that only a subset of the height components is described by a nontrivial elastic theory.

APPENDIX B: Proof for repeat lattice

In this Appendix we rigorously show that two domains of the same ideal state always differ in height by a vector of the repeat lattice, from which it follows that the coarse-grained height of any ideal state is unique modulo the repeat lattice. This is done for both cases, the 3-state Potts AFM (see Sec. 2.2) and the 4-state CPAFM model (see Sec. 3.3).

B.1 Palindromic sequences

In either case ($q = 3$ or $q = 4$), we focus on the sequence of spins $\sigma_0\sigma_1\sigma_2 \dots \sigma_{n-1}\sigma_n$ connecting two sites. We do not care which path these spins lie along, since the height difference between the first and last site depends only on the sequence as in Eq. (2.6); or, for $q = 4$, on the sequence and on the parity ϵ_0 of the initial site as in Eq. (3.5). We denote the height difference as $\Delta\mathbf{z}(\epsilon_0; \sigma_0\sigma_1\sigma_2 \dots \sigma_n)$. Now

$$\begin{aligned} \Delta\mathbf{z}(\epsilon_0; \sigma_0\sigma_1\sigma_2 \dots \sigma_{j-1}\sigma_j\sigma_{j+1} \dots \sigma_{n-1}\sigma_n) \\ = \Delta\mathbf{z}(\epsilon_0; \sigma_0\sigma_1\sigma_2 \dots \sigma_{j-1}\sigma_j) + \Delta\mathbf{z}(\epsilon_j; \sigma_j\sigma_{j+1} \dots \sigma_{n-1}\sigma_n), \end{aligned} \quad (\text{B.B.1})$$

so we shall proceed by breaking all sequences down into a few kinds of subsequence.

We call ‘palindromic’ a sequence of form $\sigma^{(0)}\sigma^{(1)} \dots \sigma^{(j-1)}\sigma^{(j)}\sigma^{(j-1)} \dots \sigma^{(1)}\sigma^{(0)}$ (with $j \geq 1$), i.e. the sequence has reflection symmetry about one spin. Of course, the corresponding spins both have the same parity. The net height change $\Delta\mathbf{z}$ of any palindromic sequence is clearly zero, since (as can be checked from the height rule definitions) $\Delta\mathbf{z}(\epsilon_i; \sigma^{(i)}\sigma^{(i+1)}) = -\Delta\mathbf{z}(\epsilon_{i+1}; \sigma^{(i+1)}\sigma^{(i)})$. (In fact, this obviously must be true since the palindromic sequence also describes a path from the initial spin back to itself.) Therefore, using (B.B.1) the net $\Delta\mathbf{z}$ of a sequence containing this palindrome is invariant if the palindrome is reduced to the single spin $\sigma^{(0)}$. Note that such a reduction keeps invariant the parity of the length of the sequence.

B.2 Three-state Potts AFM case

We are concerned with paths between sites in the same kind of domain – say, an AX domain. So we limit ourselves to paths which connect sites of the same parity. Then the corresponding sequence of spins has an even number of steps, and it begins and ends with the same Potts state A.

We can break each such sequence up into subsequences which begin and end in A; by (B.B.1) the net Δz is the sum of those of the subsequences; furthermore, we can reduce any palindromes within the subsequences without affecting this sum. Thus each term in the sum represents a palindrome-free sequence beginning and ending with A and containing no interior A's; the only such sequences are A, ABCA, and ACBA, which have Δz equal to 0, 3, and -3 , respectively. There must be an even number of three-step terms, since we chose the total sequence to have an even number of steps. Thus, finally, the net Δz is a sum of an even number of ± 3 terms, and hence is a multiple of 6, which completes the demonstration: the possible height differences Δh between two A B/C domains are precisely the integer multiples of 6.

Analogous results hold for the macroscopic height difference between any two domains of (possibly) different ideal states. For example, Eq. (2.6) for Δh between an A B/C domain and a C/A B domain is simply that for some spin sequence of odd length that begins with A and ends with B. We can always decompose such a sequence into two subsequences, the first beginning and ending with A and the second beginning with A, ending with B and containing no interior A's. The first sequence has $\Delta z \equiv 0 \pmod{6}$ and the second subsequence can be reduced to the palindrome-free AB, for which $\Delta z = 1$. Hence the macroscopic height difference between an A B/C domain and a C/A B domain is always congruent to 1 (mod 6).

B.3 Four-state CPAFM case

The method of proof for the 3-state model must be extended in this case since there are now infinitely many palindrome-free sequences beginning and ending with A and containing no interior A's. To address this, let us first replace every spin $\sigma^{(k)}$ which is not an A spin by the palindrome $\sigma^{(k)}A\sigma^{(k)}$; clearly this doesn't change $\Delta\mathbf{z}$. In this fashion the entire sequence is broken into short subsequences and we can write $\Delta\mathbf{z}$ as the sum of terms of the form $\Delta\mathbf{z}(\epsilon, AXA)$ or $\Delta\mathbf{z}(\epsilon, AXYA)$, where X and Y are spins distinct from each other and from A. The palindromes AXA are produced whenever the original sequence had an A; such palindromes can be reduced leaving only the 3-step terms. Moreover, since they involve an odd number of steps, the parity must alternate between $\epsilon = 1$ and $\epsilon = -1$ in successive terms. Thus, $\Delta\mathbf{z}$ is the sum of terms of form $\Delta\mathbf{z}(1, AXYA) + \Delta\mathbf{z}(-1, AX'Y'A)$, where X and Y need not differ from X' and Y' . Constructing all possible terms of that form (using Table 2), one finds that $\Delta\mathbf{z}$ must be a linear combination of the six vectors $(4, 0, 0)_E \pm (0, 6)_O$, $(0, 4, 0)_E \pm (-6, 0)_O$, and $(0, 0, 4)_E \pm (6, -6)_O$, which are the same as those in Eq. (3.6). (Conversely, it is also obvious that for any such linear combination, a sequence exists.) Clearly the Bravais lattice generated by linear combinations of these vectors is the 'repeat lattice' for the 4-state CPAFM.

APPENDIX C: Ergodicity of the update move

Ergodicity requires that it be possible to apply successive update moves to any allowed configuration to obtain any other allowed configuration. Since the update move we used is reversible, it is sufficient to show that any starting configuration can be converted into the configuration with all A's on the even sublattice and all B's on the odd sublattice.

Also, note that in an XY -cluster all the X's are on one sublattice and all the Y's are on the other sublattice. A corollary is that if a site with spin X and a site with spin Y are in the same sublattice, then the two sites are not in the same XY -cluster. Similarly, if two sites both have spin X but are in different sublattices, then they are in different XY -clusters for all $Y \neq X$.

Now, consider an arbitrary initial configuration of spins. Pick any site and note its spin, X, and which sublattice it is in. If the chosen site is in the even sublattice and $X \neq A$, then interchange spins $X \leftrightarrow A$ within the XA -cluster containing the site; if the chosen site is in the odd sublattice and $X \neq B$, then interchange spins $X \leftrightarrow B$ within the XB -cluster containing the site; otherwise, do not perform an update move. In this way we set the spin on the chosen site to the value it takes in the 'target' configuration, which consists of A's on the even sublattice and B's on the odd sublattice.

In the same manner, proceed one by one through the rest of the sites in the lattice, performing the appropriate update move, if necessary, to set the site's spin to the value it takes in the target configuration. The corollaries mentioned above ensure that once a site's spin has been set to its target value, it is not altered by the subsequent update moves used to set other spins to their target values; for, a site whose spin is set to its target value and a site whose spin is not set to its target value can never be in the same update cluster. For this reason, at the end of the process the target configuration has been reached. Therefore, the update move is ergodic.

Note that this proof is valid whether or not periodic boundary conditions are used. In the case of periodic boundary conditions, however, it has been implicitly assumed that the

target configuration exists, which requires that the lattice have even numbers of rows and columns. As mentioned at the beginning of Sec. 4.1, this requirement is a natural one to include in any simulation since it is necessary for the ideal states of the model to exist.

Also, note that this proof is equally valid for a standard (nonconstrained) Potts AFM so long as ‘cluster’ is appropriately redefined. In fact, the arguments here prove the ergodicity of the update move for any bipartite lattice since the target ‘AB’ configuration exists. This does not contradict the statement of Lubin and Sokal (1993) that the algorithm is not ergodic on $3m \times 3n$ lattices when m and n are relatively prime because we require that m and n both be even.

List of Figures

Fig. 1. (a) A ground state of the 3-state Potts AFM. On the left side is a portion of the A B/C ideal state; in the middle, a portion of the AB state (not an ideal state); on the right, a random state. (b) The corresponding height configuration. (Note that the heights are well-defined only after the height at one site is fixed.)

Fig. 2. (a) The six ideal states of the 3-state Potts AFM arranged in a circle, with heights as indicated. (b) The ‘ideal-states’ graph, with repeat distance 6, and operator components \mathbf{m}^s and \mathbf{m} shown as a function of h . The operator P (not shown) would alternately take values $+\frac{1}{2}$ and $-\frac{1}{2}$.

Fig. 3. (a) Portion of a ground state of the 4-state CPAFM. The left portion shows the A B/C/D ideal state, while the right portion (separated by a vertical dashed line) shows a random state. (b) The corresponding configuration of even height component h_1 . (c) The corresponding configuration of odd height component h_4 .

Fig. 4. (a) A ‘roof’ starting configuration for the 3-state Potts AFM. The height variables in each quadrant have a (different) uniform tilt, which is the largest possible. This is also a valid ‘roof’ configuration for the 4-state CPAFM model. (b) The corresponding configuration of even height component h_1 in the 4-state CPAFM. (c) The corresponding configuration of odd height component h_4 in the 4-state CPAFM.

Fig. 5. Plot of $|\mathbf{q}|^2 \langle |h(\mathbf{q})|^2 \rangle$ vs. $|\mathbf{q}|^2$ for the 3-state simulation (size 64×64). The (nearly) horizontal line shows the best linear fit to the data.

Fig. 6. Plot of $|\mathbf{q}|^2 \langle |h_1(\mathbf{q})|^2 \rangle$ vs. $|\mathbf{q}|^2$ (log-log) for the 4-state CPAFM model.

Fig. 7. This graph overlays plots of $|\mathbf{q}|^2 \langle |h_1(\mathbf{q})|^2 \rangle$ and of $|\mathbf{q}|^2 \langle |h_4(\mathbf{q})|^2 \rangle / 3$, against $|\mathbf{q}|^2$ for the 4-state CPAFM model showing they cannot be distinguished. (Data are from a 64×64 lattice and, for clarity, only $\mathbf{q} \parallel (\pm 1, \pm 1)$ have been included.)

Fig. 8. Scaling plot overlaying data on $|\mathbf{q}|^2 \langle |h_1(\mathbf{q})|^2 \rangle$ vs. $|\mathbf{q}|^2$ for the 4-state CPAFM model, for various system sizes. (The largest $|\mathbf{q}|$ values have been omitted.)

Fig. 9. Mean square total magnetization $\langle |\mathbf{M}|^2 \rangle$ vs. system size N (log-log plot). The line is the fit $\langle |\mathbf{M}|^2 \rangle \sim N^{1.85}$.

Fig. 10. A 32×32 portion of a typical configuration found in simulation of the $L = 64$ system.

(a)

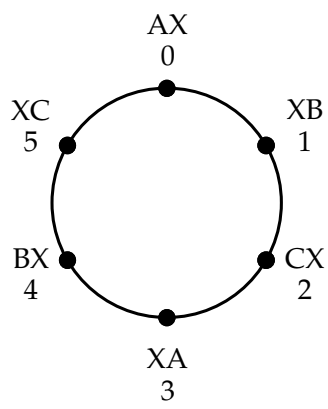
A C A B A B A B | C B C B A B A B
B A B A C A B A | B A B C B C B C
A C A C A C A B | A B C A C A C A
C A B A C A B A | B A B C A B A C
A B A B A C A C | A B C A B C B A
C A B A B A B A | B A B C A B A C
A B A C A C A B | C B A B C A C B
B A C A C A C A | B A C A B C B A

(b)

2 1 2 3 2 3 2 3 | 4 3 4 3 2 3 2 3
3 2 3 2 1 2 3 2 | 3 2 3 4 3 4 3 4
2 1 2 1 2 1 2 3 | 2 3 4 5 4 5 4 5
1 2 3 2 1 2 3 2 | 3 2 3 4 5 6 5 4
2 3 2 3 2 1 2 1 | 2 3 4 5 6 7 6 5
1 2 3 2 3 2 3 2 | 3 2 3 4 5 6 5 4
2 3 2 1 2 1 2 3 | 4 3 2 3 4 5 4 3
3 2 1 2 1 2 1 2 | 3 2 1 2 3 4 3 2

Figure 1:

(a)



(b)

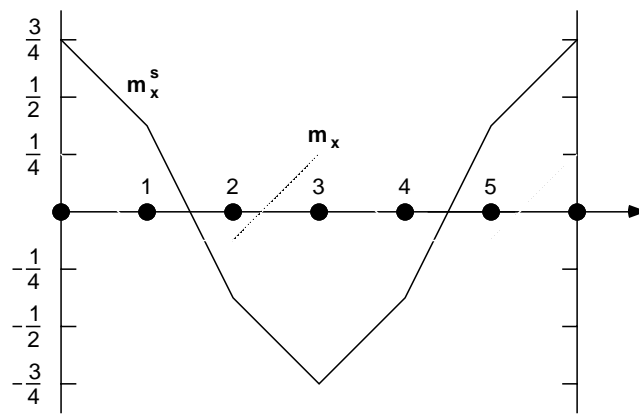


Figure 2:

(a)

A C A D | A B C A
B A B A | C A B C
A C A B | A C A B
C A D A | D A D A
A B A C | A B A C
D A D A | B C B A
A C A B | D B D B
B A C A | B A B C

(b)

2 3 2 1 | 2 2 1 0
2 2 2 2 | 3 2 2 1
2 3 2 2 | 2 3 2 2
3 2 1 2 | 1 2 1 2
2 2 2 3 | 2 2 2 3
1 2 1 2 | 2 1 2 2
2 3 2 2 | 3 2 3 2
2 2 3 2 | 2 2 2 1

(c)

2 1 2 1 | 2 4 5 4
4 2 4 2 | 1 2 4 5
2 1 2 4 | 2 1 2 4
1 2 1 2 | 1 2 1 2
2 4 2 1 | 2 4 2 1
1 2 1 2 | 4 5 4 2
2 1 2 4 | 5 4 5 4
4 2 1 2 | 4 2 4 5

Figure 3:

(a)

A B C A B A C B A C
B C A B C B A C B A
C A B C A C B A C B
A B C A B A C B A C
B C A B C B A C B A
A B C A B A C B A C
C A B C A C B A C B
B C A B C B A C B A
A B C A B A C B A C
C A B C A C B A C B

(b)

6 6 5 4 4 4 5 6 6 7
6 5 4 4 3 4 4 5 6 6
5 4 4 3 2 3 4 4 5 6
4 4 3 2 2 2 3 4 4 5
4 3 2 2 1 2 2 3 4 4
4 4 3 2 2 2 3 4 4 5
5 4 4 3 2 3 4 4 5 6
6 5 4 4 3 4 4 5 6 6
6 6 5 4 4 4 5 6 6 7
7 6 6 5 4 5 6 6 7 8

(c)

1 3 4 3 1 3 4 3 1 0
3 4 3 1 0 1 3 4 3 1
4 3 1 0 1 0 1 3 4 3
3 1 0 1 3 1 0 1 3 4
1 0 1 3 4 3 1 0 1 3
3 1 0 1 3 1 0 1 3 4
4 3 1 0 1 0 1 3 4 3
3 4 3 1 0 1 3 4 3 1
1 3 4 3 1 3 4 3 1 0
0 1 3 4 3 4 3 1 0 1

Figure 4:

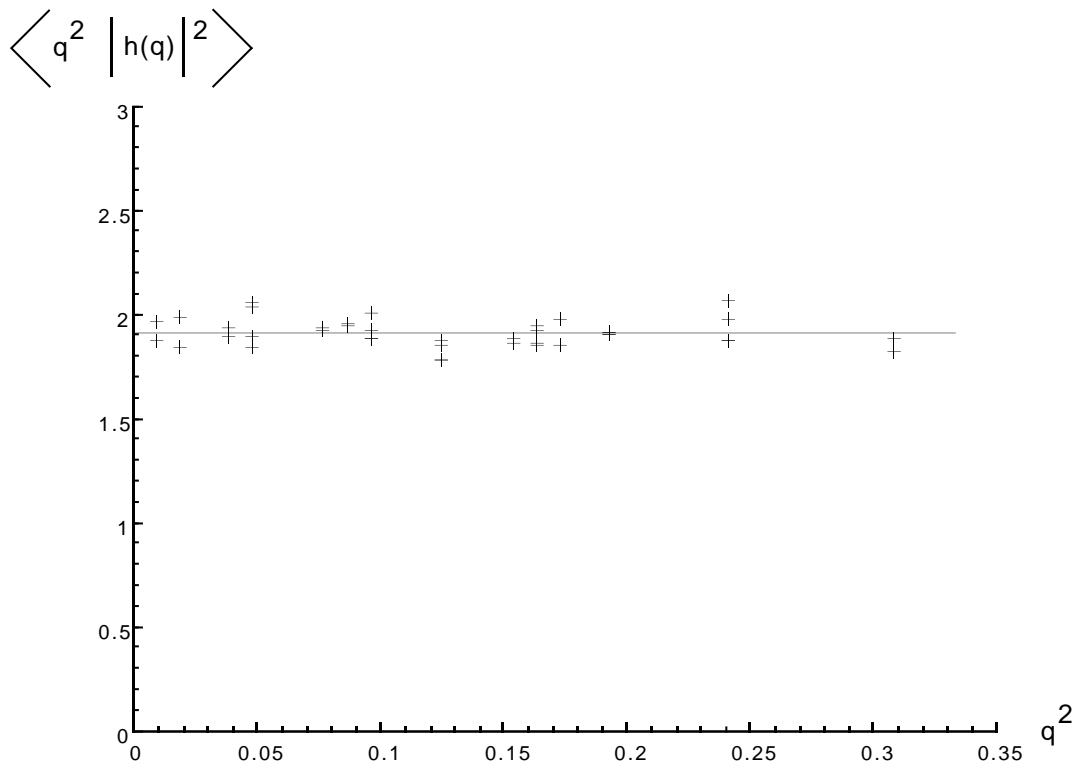


Figure 5:

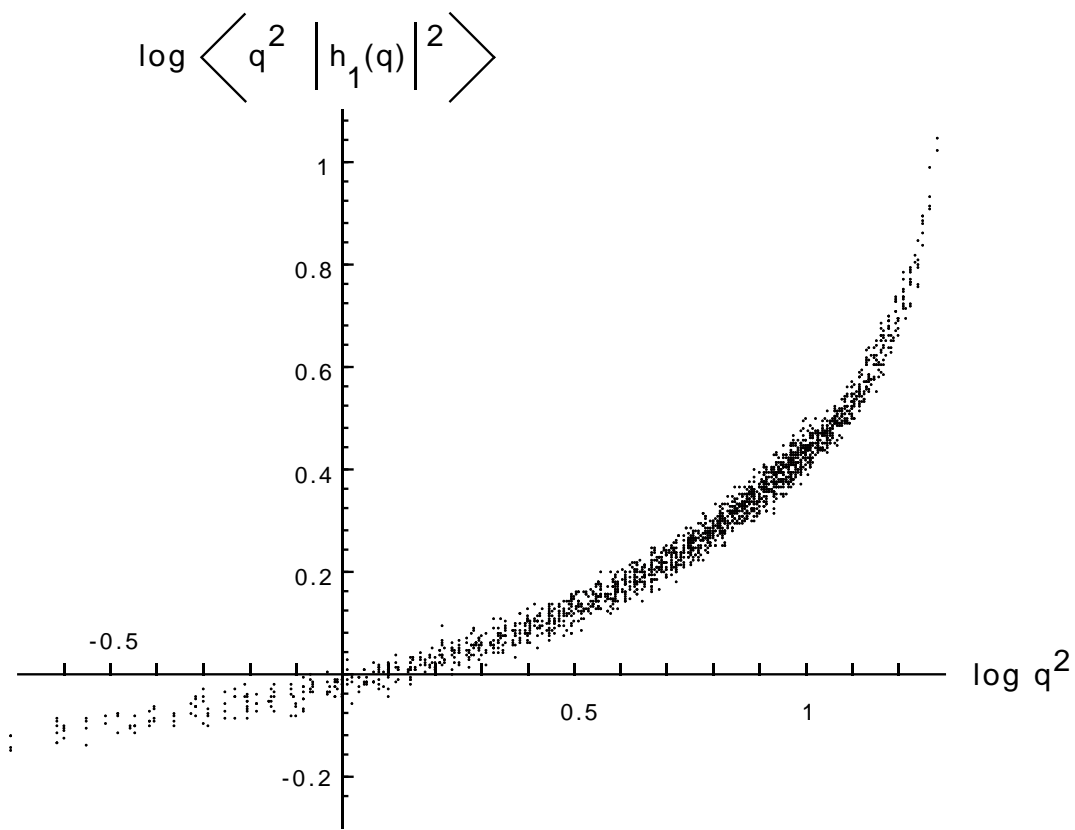


Figure 6:

$$\left\langle q^2 \left| h_1(q) \right|^2 \right\rangle$$

$$\left\langle \frac{q^2}{3} \left| h_4(q) \right|^2 \right\rangle$$

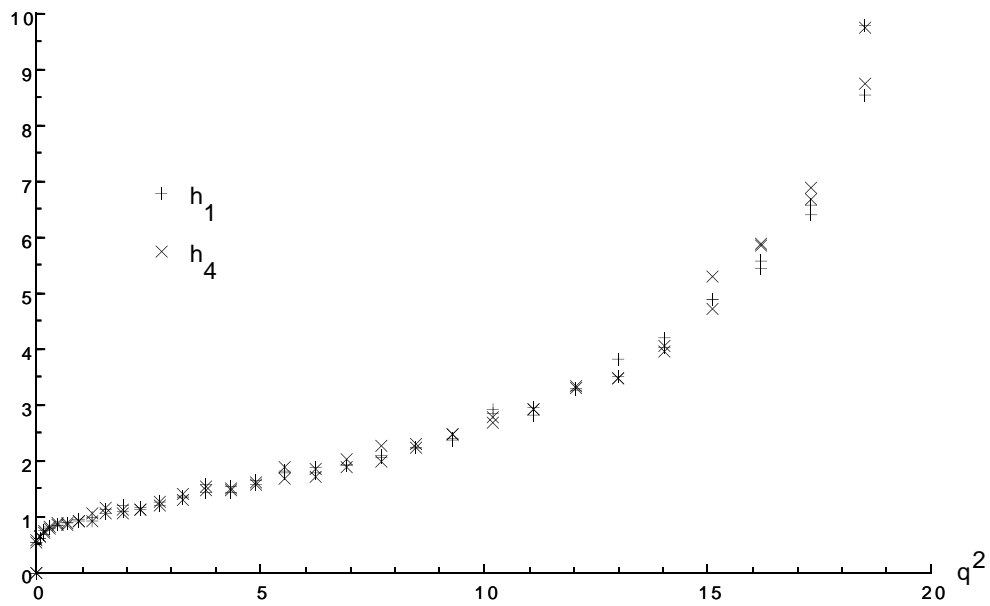


Figure 7:

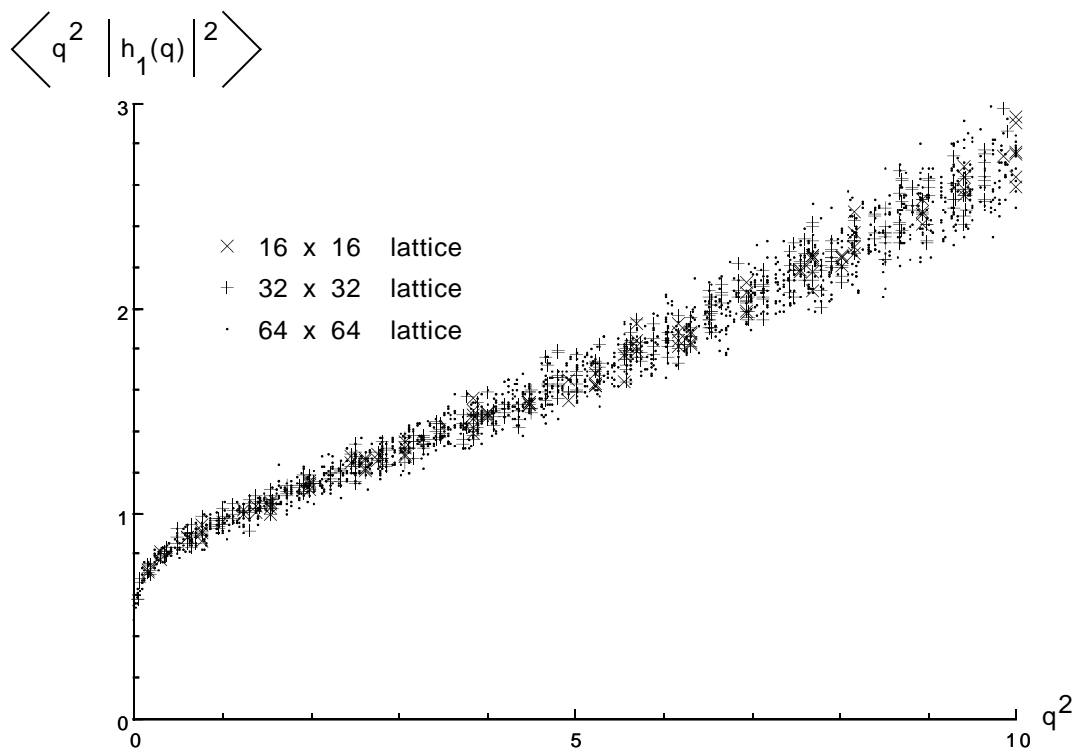


Figure 8:

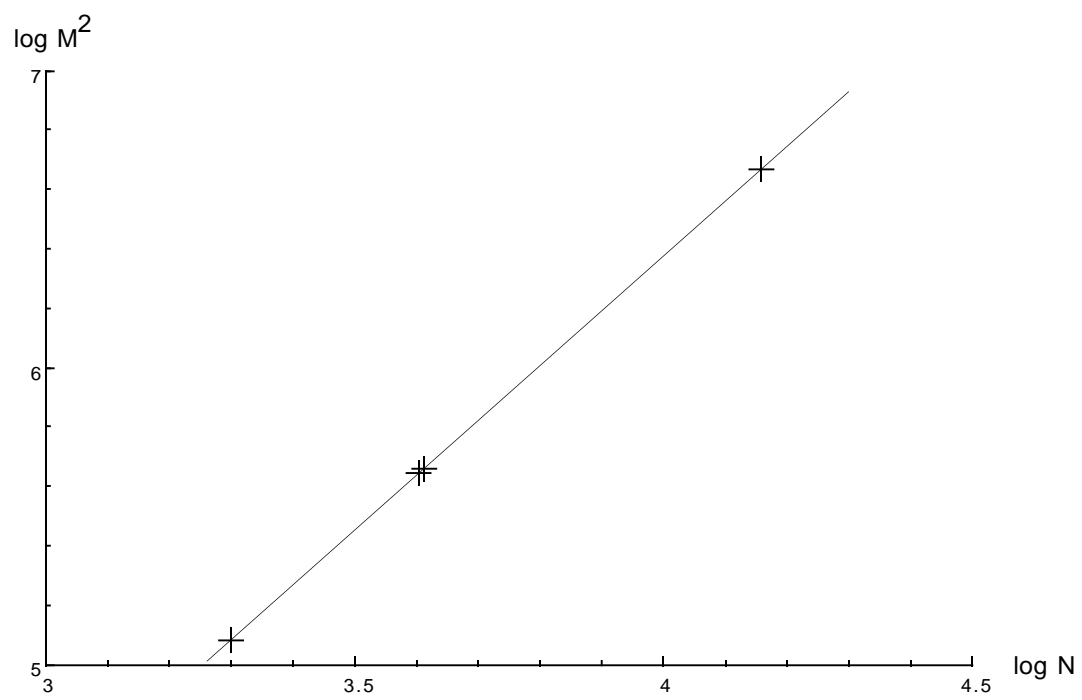


Figure 9:

A D A C A B A B C B A D C D B D B D A C A D A B A C A C A B A D
D A C A C A B D B A B A D B A B D A C A D C D A B A B A B C B A
A C A B A B A B C B A C A D B A B D A D C B C D A C A D A B A C
D A C A D A B A B A C A C A D B C B D A D C B C D A C A C A C A
C D A D A B A C A C A C B C A D B D A D C D C D A D A C A B A B
D A B A B A D A D A B A C A D B D B D C D A D A D A C D C A B A
A D A B A D A D A C A D A D A D A D B D A D A D B D A C A D A D
D A C A B A B A D A D C D A D C D B D B D B D B D C D A D A D A
A B A B A D A C A D B D C D C D B A B D B D B D C D A C A B A B
D A D A B A B A B A D B D A D B D B A B D A D B D A C A C A C A
A C A D A B A D A D A D C D C D B D B D A B A D B D A C A C A C
C A C A B A D A B A B A D A D A D A D B D A C A D A C A B A B A
A D A C A C A D A B C B A C A B A B A D A B A B A C B C A C A D
C A C A B A D A D A B A B A D A B A D A C A B A D A C A B A B A
A D A D A C A D A B A C A C A D A D A D A D A D A B A D A D A B
D A B A B A D A B A B A B A C A C A B A D A D A B C B A B A B C
A C A C A D A B A B A D A C A B A D A B A B A B C B D B A B A B
C A C A B A B A C A D B D A C A D A B A B A B A B A B C B A B A
A B A B A C A C A D A D A B A B A D A B D B A B A D A B D B C B
B A B A C A D A B A B A D A B A C A D A B A C A B A B A B C B A
D B A B A D A C A C A C A B A C A B A D A C A B C B C B D B A D
B D B A D A C A B A B A B A D A C A D A C A C A B D B C B C B A
D B C B A B A B D B A B A B A B A B A C A C A D A B A B D B C B
C D B A B A B D B D B A B D B A B A C A B A D A B C B D B D B D
D B C B A D A B C B C B C B A D A C A C A D A C A B A B C B D B
B C B A C A C A B D B A B A D B D A D A C A B A D A B C B A B C
C B C B A D A D A B A B A D B D C D B D A B A B A B D B C B D B
B D B A C A D A C A C A D A D A D C D C D A D A D A B D B C B C
D B D B A D A C A B A B A C A D B D A D C D A B A D A B C B D B
B D B C B A C A C A D A B A D A D C D A D A D A B A C A B D B A
A B A B A B A D A C A D A D C D C D A D A C A B A B A B D B A B
B A B C B D B A D A D B D A D A D A C A B A D A D A D A B D B A

Figure 10:

List of Tables

Table 1. Rules for height steps.

Table 2. Height differences for three-spin and four-spin strings of spins (returning to the first spin state)

Spin pair	$\Delta \mathbf{z}$
AB	$(0, 1, -1)_{\text{E}} + \epsilon(2, -1)_{\text{O}}$
AC	$(1, 0, 1)_{\text{E}} + \epsilon(-1, 2)_{\text{O}}$
AD	$(-1, -1, 0)_{\text{E}} + \epsilon(-1, -1)_{\text{O}}$
BC	$(-1, 1, 0)_{\text{E}} + \epsilon(-1, -1)_{\text{O}}$
BD	$(1, 0, -1)_{\text{E}} + \epsilon(-1, 2)_{\text{O}}$
CD	$(0, 1, 1)_{\text{E}} + \epsilon(2, -1)_{\text{O}}$

Table 1:

Spin sequence	$\Delta \mathbf{z}$
ABCA	$(-2, 2, -2)_{\text{E}} + \epsilon(2, 2)_{\text{O}}$
ABDA	$(2, 2, -2)_{\text{E}} + \epsilon(2, -4)_{\text{O}}$
ACDA	$(2, 2, 2)_{\text{E}} + \epsilon(-4, 2)_{\text{O}}$
ACBA	$(2, -2, 2)_{\text{E}} + \epsilon(2, 2)_{\text{O}}$
ADBA	$(-2, -2, 2)_{\text{E}} + \epsilon(2, -4)_{\text{O}}$
ADCA	$(-2, -2, -2)_{\text{E}} + \epsilon(-4, 2)_{\text{O}}$
ACBDA	$(4, 0, 0)_{\text{E}} + \epsilon(0, 6)_{\text{O}}$
ABCDA	$(0, 4, 0)_{\text{E}} + \epsilon(6, 0)_{\text{O}}$
ACDBA	$(0, 0, 4)_{\text{E}} + \epsilon(-6, 6)_{\text{O}}$
ADBCA	$(-4, 0, 0)_{\text{E}} + \epsilon(0, -6)_{\text{O}}$
ADCBA	$(0, -4, 0)_{\text{E}} + \epsilon(-6, 0)_{\text{O}}$
ABDCA	$(0, 0, -4)_{\text{E}} + \epsilon(6, -6)_{\text{O}}$

Table 2: